

AD-A155 769

CASSCF (COMPLETE ACTIVE SPACE SELF CONSISTENT FIELD) -
WAVE PACKET AB INIT. (U) CALIFORNIA UNIV SAN DIEGO LA
JOLLA DEPT OF CHEMISTRY J R REIMERS ET AL. 1985
N00014-78-C-0325

1/1

UNCLASSIFIED

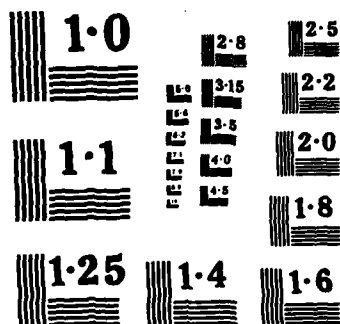
F/G 20/8

NL

END

FORMED

DEC



NATIONAL BUREAU OF STANDARDS
MICROCOPY RESOLUTION TEST CHART

① ②

Absorption of C_7H at 3000K.

Jeffrey R. Reimers and Kent R. Wilson

Eric J. Heller[#]

and

**NASA Ames Research Center
Moffett Field, California 94035**

DTIC ELECTE
JUN 24 1985
A

Current address: Chemistry Department BG-10, University of Washington, Seattle
WA 98195.

OTIC FILE COPY

little orange

EX-107
DISTRIBUTION:
Available by Codes
A-11111111
1-1-68

A1



This document has been released for public release and sale. Its distribution is unlimited.

85 5 29 112

[A(1st and 2nd Power Pi) reversible reaction X(1st and 2nd Power Sigma(4))]

ABSTRACT

The combination of *ab initio* calculation of the electronic wavefunctions with a wave packet calculation of the nuclear motion is used, within the Born-Oppenheimer approximation, to compute the vibrational and electronic absorption of a polyatomic molecule. A particular virtue of this approach is that high as well as low temperature spectra are both calculable. This method is applied to C_2H , for which the Complete Active Space Self Consistent Field (CASSCF) method is used to determine full Born-Oppenheimer potential surfaces. Using the assumption that the $A(^2\Pi) \leftarrow X(^2\Sigma^+)$ absorption can be written as the sum of the $A(^2A') \leftarrow X$ and $A(^2A'') \leftarrow X$ absorptions, the spectra are determined to 60 cm^{-1} resolution at a temperature of 3000K. As a result of the large thermal bending amplitude at 3000K, the calculated spectra are broad and have little resolved structure. Two bands are resolvable, one is due to the $A(^2A') \leftarrow X$ absorption and is centered at 5500 cm^{-1} , while the other is due to the $A(^2A'') \leftarrow X$ absorption and is centered at 9500 cm^{-1} . The dramatic blue shift of the $A(^2A') \leftarrow X$ band results from the combination of the large X state thermal bending amplitude and the high bending frequency of the $A(^2A')$ state. We also determine the X state pure vibrational absorption spectrum and show it to be of much lower intensity than the pure electronic spectrum.

I. INTRODUCTION

Small polyatomic molecules are often found in high temperature environments such as flames, stars, and shock fronts. From a knowledge of their cross-sections, we can learn much about the chemical reaction taking place and the transport processes occurring in the system. They are often difficult to observe, however, as the experimental conditions are harsh and the molecules are often very reactive, for example, free radicals. Here, we present an *ab initio* technique, which is within the Born-Oppenheimer framework, for predicting spectra of small molecules as a function of temperature. It uses a combination of the precise and efficient Complete Active Space Self Consistent Field (CASSCF) method for determining electronic wavefunctions, with a fast time-dependent wave packet technique to account for the effects of nuclear motion. These techniques are generally applicable to a large range of molecules, and may be applied to calculate spectra of samples at any temperature. Vibrational and electronic spectra of C_2H are calculated as an example application of this technique.

The ethynyl radical $\bullet C \equiv CH$ is believed to be an important species. Unassigned spectral lines in the interstellar medium¹⁻⁴ have been attributed to C_2H ; it is thought to be abundant in carbon rich stars,⁵⁻⁸ and to be important as a chemical reaction intermediate,^{9, 10} especially on Jupiter.¹¹ In the laboratory it is very difficult to produce and positively identify C_2H . Common methods of production include photolysis¹² of C_2H_2 and electric discharges^{13, 14} either in C_2H_2 or over polyacetylene.¹⁵ Recently, a summary of production methods has been given by Laufer.⁷ The most important signatures of the molecule are its four rotational lines near 87.3 GHz^{1, 12, 16, 17} and its CC stretching fundamental^{13, 18} at 1848 cm^{-1} . Jacox¹³ observed the CH stretching fundamental for C_2H trapped in an inert matrix at 14K to be at 3612 cm^{-1} . Under similar conditions Graham, Dismuke and Weltner¹² observed the lowest lying electronic transition, $A(^2\Pi) \leftarrow X(^2\Sigma^+)$, to be a poorly resolved band in the red near 10000 cm^{-1} . This band is strongly solvent dependent and in the gas phase is both observed¹⁵ and predicted¹⁹ to have its origin transition near 3600 cm^{-1} . Carrick, Merer and Curl¹⁵ have taken high resolution spectra in the 3600-4200 cm^{-1} region and have identified five vibronic levels. None of these levels were identified as the ground state CH stretching fundamental ν_1 which was presumed to be swamped in intensity by the electronic transition. Interpretation of the high resolution spectra is very difficult as there is strong Renner-Teller coupling in the A state, strong²⁰ coupling between the A and X states once the molecule bends, and strong spin-orbit coupling.

[A(1st and 2nd Power A double Prime) reversible reaction X]

Shih, Peyerimhoff and Buenker have made *ab initio* calculations of both the vertical electronic spectrum¹⁹ and the emission spectrum²¹ of C_2H . They predicted that the origin and center of the $A \leftarrow X$ absorption band should be around 4000cm^{-1} and 5800cm^{-1} , respectively. Also, they predicted that the band should show a progression in the excited state CC stretch vibration ν_3 . The majority of the excited states were predicted to have long CC bond lengths and bent equilibrium geometries, accounting for the vast differences observed between absorption and emission spectra.^{10, 21}

The vertical electronic spectral calculations of Shih, Peyerimhoff and Buenker¹⁹ predict, at 0K, the total intensity and band center of the absorption. They give only qualitative information on the bandwidth and no information on either structure within the band or on the change of band shape with temperature. Experimentally, only a few lines in the low frequency tail of the $A \leftarrow X$ absorption band have been observed in the gas phase.¹⁵ This paper describes a calculation of the principal intensity distribution of the $A \leftarrow X$ absorption band at 3000K. This is shown to be dramatically different from the 0K spectrum. High temperature information is important to combustion^{7, 10} studies, as well as to the problem of the heating of a space probe entering the Julian atmosphere.^{22, 23}

We use the Complete Active Space Self Consistent Field^{7, 10, 24, 25} (CASSCF) method to calculate the adiabatic potential surfaces, fitting this data to a functional form of the potential. Infrared and electronic spectra are then calculated using the time dependent quantum formalism of Reimers, Wilson and Heller.²⁶ In order to apply this formalism we make the assumption that the full $A(^2\Pi) \leftarrow X(^2\Sigma^+)$ absorption spectrum can be written as the sum of spectra calculated for each component of the bent A state, $A(^2A') \leftarrow X$ and $A(^2A'') \leftarrow X$. The results show, at low resolution, how the gross features of the absorption contour change shape with temperature. The main changes in the intensity distribution with increasing temperature are seen to be a blue shift due to the very high bend vibrational frequency of the $A(^2A')$ state and a broadening due to the considerable anharmonicity of the potential surfaces.

The CASSCF method^{24, 25} is chosen to generate the potential surfaces for the following reasons. First, the method employs a fixed configuration list at all geometries, thus being capable of high precision. This is an essential consideration when the potentials are to be fitted to a functional form. Second, the method leads to proper dissociation and tends to treat the surfaces with uniform accuracy even for large displacements from equilibrium. Finally, the CASSCF method is sufficiently economical to permit a large number of energy and dipole moment evaluations on both the X and A surfaces. More elaborate methods of including correlation, such as multi-reference singles plus doubles configuration interaction, would require a very large number of references to describe the entire surfaces equivalently. Selection methods, which would make the calculation feasible, tend to reduce significantly the precision of the surface.

Traditionally, spectra would be calculated by first solving the Watson Hamiltonian,²⁷ assuming adiabatic potential surfaces and no spin-orbit coupling. The extra couplings would then be included in a variational calculation and the observed energies and intensities calculated. This is an extremely ambitious calculation, as many hundreds of vibronic states contribute to the 3000K spectrum, and each of these states will have complicated PQR rotational structures. At the moment such a calculation is not feasible. Consider, by way of example, the well-studied case of the water molecule. Compared to C_2H , it has relatively low anharmonicity, yet, using conventional normal mode approaches, it is currently only possible to determine the lowest 20 vibrational levels of water accurately²⁸ (though use of local mode basis sets significantly improve this calculation²⁹).

No vibrational eigenfunctions are required in the approach of Reimers, Wilson and Heller.²⁶ Here the spectrum is given as the Fourier transform of the time correlation function obtained by evaluating the phase space average of the overlap of two gaussian

wave packets. One of these wave packets propagates on the ground potential energy surface while the other propagates on the excited potential energy surface. The frozen gaussian approximation^{26,30} to wave packet dynamics is used in all calculations, and a classical approximation²⁶ to the temperature operator is used in all calculations at nonzero temperature. Such a calculation is termed FC: here F stands for "Frozen" and C stands for "Classical". In view of all of the other approximations used in this calculation, it is felt that improving upon either of the FC approximations is not justified at this time.

All of the approximations made are insignificant for band contour calculations as the contour is determined by only the first few femtoseconds of the time correlation function. Band contour calculations are also very fast, typically requiring less than a minute of DEC VAX-780 computer time. The spectra reported here are at 60cm^{-1} resolution corresponding to a propagation time of 530fs. Non-adiabatic effects, spin-orbit coupling, wave packet deformations, etc, all affect the dynamics at long times, causing the calculated lines to be split and the intensity pattern to broaden. Clearly, 60cm^{-1} resolution is too narrow (the spin-orbit coupling alone is known to be 52cm^{-1} , for example), but it is best to present spectra which are known to be too sharp rather than spectra which are thought to be too broad. A typical calculation at this resolution takes 0.5-2.0 hours of VAX-780 computer time.

II. CALCULATION METHODS

A. *Ab Initio* Calculations

All of the X , $A(^2A')$ and $A(^2A'')$ surfaces are calculated over a large geometry range using the CASSCF method. The X state is defined over the range accessible thermally at a temperature of 3000K, while the $A(^2A')$ and $A(^2A'')$ surfaces are defined over the entire energy range accessible to trajectories starting vertically above this ground state distribution.

The CASSCF potential energy surfaces are generated using a double-zeta plus polarization (DZP) basis set of cartesian gaussian functions. For carbon we use the $[4s\ 2p]$ contraction³¹ of the $[9s\ 5p]$ Huzinaga set,³² augmented by a d function with an orbital exponent of 0.75. For hydrogen, we use the $[3s]$ contraction³³ of the $[5s]$ Huzinaga³² set, multiplied by a scale factor of 1.2 and augmented by a p function with an orbital exponent of 1.728.

In our CASSCF calculation the seven outermost valence electrons are correlated in seven active orbitals - five of a' symmetry and two of a'' symmetry. All calculations (even at C_{2v} geometries) are carried out in C_s symmetry to ensure that no discontinuities arise on the A surfaces upon bending. Making all possible arrangements of the seven electrons in the seven orbitals consistent with spin and symmetry restrictions results in 404 configurations for the $A(^2A')$ state and 380 configurations for the $A(^2A'')$ state. Calculations with both smaller and larger active spaces indicates that these CASSCF calculations are reasonably well converged.

The CASSCF dipole moment surface is used to compute the infrared spectrum of the $X(^2\Sigma^+)$ ground state. Analogous CASSCF calculations on the ozone molecule³⁴ produce intensities for the fundamental and lowest combination and overtone bands that are in excellent agreement with experiment. Further improvement in the dipole moment function would require the inclusion of a diffuse d function in the basis set, as well as a more extensive treatment of the electron correlation.

Since the CASSCF wavefunctions for the X and A states are defined in different orbital bases, we can not use these wavefunctions to deduce the electronic transition moment functions. Instead we use transition moments based upon CI wavefunctions defined in terms of the ground state Hartree-Fock orbitals. The transition moments are rather insensitive to electron correlation owing to the fact that the dominant

configurations of the X and A states differ by one spin orbital. Hence, the transition moments are calculated using only small CI wavefunctions with selection based on the magnitude of the diagonal hamiltonian matrix elements. The calculated oscillator strength at the equilibrium geometry is in excellent agreement with more extensive singles plus doubles CI treatments as well as with the results of Shih Peyerimhoff and Buenker.¹⁹ Note that in this calculation only three cuts through the full transition moment profile are determined.

B. Spectroscopic Analysis

The spectroscopic programs are very general and can be written in a variety of co-ordinate systems. Typically they are written in cartesian co-ordinates. These are conceptually the simplest and require no separation of rotational and vibrational variables. For proteins, liquids and moderate sized molecules they are clearly the best possible co-ordinates but, for triatomic molecules, they have the disadvantage of containing three times the number of variables that a purely vibrational set of co-ordinates would contain. Initially we planned to run thawed gaussians,^{26, 35} for which this problem is accentuated as the second derivatives of the potential surface are then required. Also thawed gaussians require special treatment to include rotational degrees of freedom.^{36, 37} Finally, cartesian co-ordinate potential functions require a large number of square root and trigonometric function evaluations, which significantly slow the programs.

A common alternative to cartesian co-ordinates is valence co-ordinates (bond lengths and angles). Their use introduces the rigid rotor approximation. The potential energy then takes a much simpler form, at the expense of complicating the kinetic energy operator. Another approach is to use normal co-ordinates. They again restore the kinetic energy operator to a simple form but are usually regarded as poor variables in which to expand a potential surface. Here a simple non-linear transformation is used to construct, from the normal co-ordinates, a new set of co-ordinates which closely resemble the valence co-ordinates. The spectroscopic programs can thus be written entirely in normal co-ordinates. In this approach a large part of the anharmonicity of the spectra is attributed to the intrinsic curvilinear nature of the molecular potential surface. This is equivalent to the unphysical concept of "kinetic energy anharmonicity", which is commonly referred to in the literature of calculations that use valence co-ordinates.

Using normal co-ordinates, the basic formalism²⁶ for the infrared or electronic cross section $\sigma_T(\omega)$, at temperature T , becomes the Fourier transform

$$\sigma_T(\omega) = \frac{2\pi\omega}{3\hbar c} (1 - e^{-\beta\hbar\omega}) \int_{-\infty}^{\infty} C_T(t) e^{i\omega t} dt \quad (2.1)$$

of the time correlation function

$$C_T(t) = Q^{-1} \int_{-\infty}^{\infty} d^n q_0 d^n p_0 \langle \chi_{q_0 p_0} | e^{-\beta H_i} e^{iH_i t / \hbar} \mu^* e^{-iH_f t / \hbar} \mu | \chi_{q_0 p_0} \rangle \quad (2.2)$$

where $\beta = (kT)^{-1}$, k is Boltzmann's constant, c is the speed of light, Q is the quantum partition function,

$$Q = \int_{-\infty}^{\infty} d^n q_0 d^n p_0 \langle \chi_{q_0 p_0} | e^{-\beta H_i} | \chi_{p_0 q_0} \rangle, \quad (2.3)$$

$|\chi_{p_0 q_0}\rangle$ is a gaussian wave packet initially centered at position q_0 and momentum p_0 , μ is the dipole or transition moment operator, and H_i and H_f are the initial (X) and final (A) state hamiltonians, respectively. Here we take q_0 as a vector of dimensionless normal co-ordinates and p_0 as their conjugate momenta. The classical temperature approximation²⁶ replaces the operator $e^{-\beta H_i}$ by the number $e^{-\beta E_i}$ where E_i is the classical

energy of the trajectory. This approximation arises by making a Taylor expansion, in powers of β , of the effect of the quantum operator on the wavefunction and then retaining only the leading term. It reduces the full partition function to the classical partition function,

$$Q = \int_{-\infty}^{\infty} d^n q_0 d^n p_0 e^{-\beta E}, \quad (2.4)$$

and allows the integrand in equation (2.2) to be written as Boltzmann weighted overlap $e^{-\beta E_i} \langle \Phi_i | \Phi_f \rangle$ where

$$| \Phi_i \rangle = \mu e^{-iH_i t / \hbar} | \chi_{q_0 p_0} \rangle \quad (2.5)$$

and

$$| \Phi_f \rangle = e^{-iH_f t / \hbar} \mu | \chi_{q_0 p_0} \rangle. \quad (2.6)$$

Equation (2.5) is interpreted as propagating the wave packet on the initial (X) potential surface to time t and then then operating upon the wave function with the dipole moment operator, while equation (2.6) is interpreted as propagating, on the final (A) state, the result of the dipole moment operating on the wave packet.

In this paper we use the frozen gaussian approximation³⁰ to propagate the wave packets. This constrains the width of the gaussian function to be constant in time. The center of the gaussian, initially p_0 and q_0 , then moves according to Hamilton's equations of motion, and the wave packet's phase contains a term reflecting the classical action as well as a zero point motion correction term. It is thus no more difficult to implement than is classical molecular dynamics and yet is an approximation which retains most of the essential features of quantum mechanics. Tunneling can not be directly accounted for as this demands that the wave packet splits into pieces. Features that are retained by this approach include barrier penetration, the Heisenberg uncertainty principle, zero point motion, interference effects and basic operator commutation relationships.

For linear triatomic molecules such as C_2H , there are eight phase space (position and momentum) variables to integrate over in equations (2.2)-(2.3). These integrals are evaluated numerically using a product Gauss-Hermite quadrature.³⁸ This quadrature is accelerated by only running trajectories with significant weight and by transforming to variables which better reflect the X potential surface.

The high temperature formalism presented here requires no adaptation to calculate spectra at 0K. At this temperature the classical phase space available is just one point, and the gaussian wave packet centered on this point is just the harmonic approximation to the ground state wavefunction. This formalism thus reduces to the eigenstate formalism of low temperature wave packet dynamics.³⁹ The classical approximation is thus accurate at both low temperatures ($kT/\hbar\omega < 0.5$) and high temperatures ($kT/\hbar\omega > 5$). At 3000K, the vibrations of C_2H fall into the intermediate region with $kT/\hbar\omega = 0.6, 1.1$ and 4.2 for the bend (ν_2), CC stretch (ν_3) and CH stretch (ν_1) vibrations, respectively.

III. FITTING THE AB INITIO DATA

A. Functional Form of the Potentials

The CASSCF data for each state $S = X, A(^2A')$ or $A(^2A'')$ are fitted to two potential functions. Both of these functions have the same form but they are written as functions of different position variables. One function, $V_v^{[S]}(\Delta\mathbf{r})$, is a function of $\Delta\mathbf{r} \equiv \{\Delta r_{CH}, \Delta\theta, \Delta r_{CC}\}$, the change in the valence co-ordinates $\mathbf{r} \equiv \{r_{CH}, \theta, r_{CC}\}$ from the X state equilibrium geometry $\mathbf{r}^{[X]} \equiv \{r_{CH}^{[X]}, \pi, r_{CC}^{[X]}\}$, where r_{CH} and r_{CC} are the CH

and CC interatomic distances, respectively, and θ and π are the CCH bond angle and its equilibrium value, respectively. The other function, $V_n^{[S]}(\mathbf{q})$, is a function of \mathbf{q} , a set of dimensionless normal co-ordinates of the X state, $\mathbf{q} \equiv \{q_1, q_2, q_3\}$ where q_1 is predominately the CH stretch, q_2 is the bend and q_3 is predominately the CC stretch. Since C_2H is linear, the bend co-ordinates $\Delta\theta$ and q_2 have two degenerate components. If ϕ is an angle which specifies the angle between the plane of a bent molecule and the plane perpendicular to the original molecular axis then we take these components as the cartesian co-ordinates

$$x \equiv \Delta\theta_a = \sin\Delta\theta \cos\phi \quad \text{and} \quad y \equiv \Delta\theta_b = \sin\Delta\theta \sin\phi \quad (3.1)$$

and the normal co-ordinates

$$q_{2a} = q_2 \cos\phi \quad \text{and} \quad q_{2b} = q_2 \sin\phi. \quad (3.2)$$

Note that the potentials are cylindrically symmetric and independent of ϕ . The potentials $V_v^{[S]}(\Delta\mathbf{r})$ are written as functions of $\Delta\theta$ rather than $\sin\Delta\theta$ as $\Delta\theta$ has superior boundary properties at large θ . Only $V_n^{[S]}(\mathbf{q})$ are used in trajectory calculations. The $V_v^{[S]}(\Delta\mathbf{r})$ surfaces are presented for comparison.

The valence co-ordinate potentials $V_v^{[S]}(\Delta\mathbf{r})$ are written in a form containing 27 free parameters. Removing the superscript [S] for clarity, this form is written as

$$V_v^{[S]}(\Delta\mathbf{r}) = V_0 + D_{HH} x_h^2 + D_{HC} x_h x_c + D_{CC} x_c^2 + D_B (x_b - 1) + E_B (x_b^{-1} - 1) \quad (3.3)$$

where

$$x_h = 1 - \exp(-\alpha_H \delta_H), \quad (3.4)$$

$$x_c = 1 - \exp(-\alpha_C \delta_C), \quad (3.5)$$

$$x_b = \exp(\alpha_B b^2), \quad (3.6)$$

$$\alpha_H = \alpha_0^H + \alpha_H^H h + \alpha_C^H c + \alpha_{BB}^H b^2, \quad (3.7)$$

$$\alpha_C = \alpha_0^C + \alpha_H^C h + \alpha_C^C c + \alpha_{BB}^C b^2, \quad (3.8)$$

$$\alpha_B = \alpha_0^B + \alpha_H^B h + \alpha_C^B c + \alpha_{BB}^B b^2, \quad (3.9)$$

$$\delta_H = h + D_{HH} h + D_{HC} c + \delta_{BB}^H b^2, \quad (3.10)$$

$$\delta_C = c + \delta_H^C h + D_{CC} c + \delta_{BB}^C b^2, \quad (3.11)$$

$$E_B = E_0^B + E_C^B c + E_{CC}^B c^2, \quad (3.12)$$

and the displacements from the equilibrium geometry of state S are given by

$$h = \Delta r_{CH} - (r_{CH}^{[S]} - r_{CH}^{[X]}), \quad (3.13)$$

$$c = \Delta r_{CC} - (r_{CC}^{[S]} - r_{CC}^{[X]}), \quad (3.14)$$

and

$$b^2 = (\Delta\theta)^2 \quad (3.15)$$

where $r_{CH}^{[S]}$ and $r_{CC}^{[S]}$ are the equilibrium bond lengths of state S.

The stretch potentials are basically Morse functions. Due to symmetry, the bend potential must be an even function of $\Delta\theta$ and we find it convenient to write this as a function of $(\Delta\theta)^2$. The basic form used for the bend potential is a combination of a gaussian and a rising exponential. It is flexible enough to allow the equilibrium geometry to be non-linear, if necessary, and fits the C_2H surfaces much better than does

potential surfaced based upon Taylor expansions. Other terms are added to these basic functions to allow them to change curvature slightly at locations away from equilibrium.

Many other functional forms of this potential have been tested and found to be unsatisfactory. Taylor expansion type potentials, including the potentials of Carney, Curtiss and Langhoff²⁸ (an expansion in the Simon-Parr-Finlan coordinate⁴⁰ $\Delta r / r$) and a generalized Hoffaker potential⁴¹ (an expansion in the Morse variable $1 - e^{-a\Delta r}$) are too flexible. They are difficult to control as their basic shape can change rapidly over short distances producing nasty saddle points at relatively low energies. The function used here is not as flexible as these forms and its saddle points tend to be at high energies and outside the region of the potential being fitted. It still has sufficient flexibility to interpolate the potential surface accurately.

Valence co-ordinates reflect the shape of the potential surface much better than the normal co-ordinates, which are just the tangential components of the valence co-ordinates at the equilibrium geometry. The transformation from normal to valence co-ordinates has been specified up to third order by Hoy, Mills and Strey.⁴² Our approach is to include only the linear and dominant non-linear terms thus generating from the normal co-ordinates a new set of co-ordinates $s \equiv \{s_H, s_B, s_C\}$ (where again $s_{BA} = s_B \cos \phi$ and $s_{BB} = s_B \sin \phi$) that closely resemble the valence co-ordinates Δr . These are also a good set of variables in which to expand the potential, and are defined as:

$$s_H = L_{HH} q_1 + L_{HC} q_3 + L_{HBB} q_2^2 + L_{HBBBB} q_2^4, \quad (3.16)$$

$$s_C = L_{CH} q_1 + L_{CC} q_3 + L_{CBB} q_2^2 + L_{CBBBB} q_2^4, \quad (3.17)$$

$$s_B^2 = L_{BB}^2 q_2^2 + L_{BBBBB} q_2^4. \quad (3.18)$$

The normal co-ordinate potentials $V_n^{[S]}(q)$ are defined in an identical fashion to the valence co-ordinate potential, except that s_H , s_B^2 and s_C replace Δr_{CH} , $(\Delta \theta)^2$ and Δr_{CC} , respectively, in equations (3.13)-(3.15).

In the equations (3.16)-(3.18) the five non-linear L terms are treated as free parameters and are refined along with the potential constants. The five linear L terms define the direction and length of the dimensionless normal co-ordinates q . If q are to be the normal co-ordinates of $V_n^{[X]}(q)$, then the linear terms are dependent upon the other force constants.

B. Fitting the Potential Co-efficients

The potential coefficients are obtained by refining their values to minimize the error in the fitted potential V_{FIT} according to

$$\chi^2 = \sum_n \frac{(V_{FIT} - V_{CASSCF})^2}{V_{CASSCF} + 10 \text{ cm}^{-1}} \quad (3.19)$$

where the sum is over the *ab initio* CASSCF data points. This form of the error function is superior to a least squares form as it does not over emphasize the high energy points. For the X state potential energy surfaces all of the force constants are adjusted simultaneously to fit all of the CASSCF data. For the A state surfaces a different approach is taken and the stretch-only force constants are fitted to the linear data points only. All of the A surfaces thus have the same stretching potential. There are four different bending potentials: for each of the two components of the A state there are two functions generated, one in the valence co-ordinates and the other in the normal co-ordinates.

In Table I the potential constants are given and in Table II the accuracy of the fits are summarized. Table II gives, for each of the seven fits made, the total number of

E I. Potential Coefficients.

Constant	$V_n^{[X]}(q)$	$V_n^{[A(2A')]}(q)$	$V_n^{[A(2A'')]}(q)$	$V_v^{[X]}(\Delta r)$	$V_v^{[A(2A')]}(\Delta r)$	$V_v^{[A(2A'')]}(\Delta r)$
$\tau_{CH}/\text{\AA}$	1.056180	1.059800	1.059800	1.056180	1.059800	1.059800
$\tau_{CC}/\text{\AA}$	1.232760	1.314430	1.314430	1.232760	1.314430	1.314430
$L_{HBB}/\text{\AA}$	-0.148763	-0.380053	0.068499			
${}^H_{HBBB}/\text{\AA}$	-0.049642	-0.052920	-0.330783			
$L_{CBB}/\text{\AA}$	-0.004142	-0.005807	-0.008128			
${}^C_{CBBB}/\text{\AA}$	0.001944	-0.002816	-0.003152			
$L_{BBBB}/\text{\AA}$	0.011084	-0.003409	0.005216			
$\alpha_0^H/\text{\AA}^{-1}$	1.995370	1.790790	1.790790	1.737230	1.790790	1.790790
$\alpha_H^H/\text{\AA}^{-2}$	0.383248	-0.001382	-0.001382	-0.047890	-0.001382	-0.001382
$\alpha_C^H/\text{\AA}^{-2}$	-0.292976	0.190334	0.190334	-0.045747	0.190334	0.190334
$\alpha_{BB}^H/\text{\AA}^{-1}$	-0.906130	-0.746859	-0.755775	-0.071663	-0.015817	-0.053669
$\alpha_0^C/\text{\AA}^{-1}$	1.848800	1.973590	1.973590	1.918900	1.973590	1.973590
$\alpha_H^C/\text{\AA}^{-2}$	0.023466	-0.475799	-0.475799	0.016937	-0.475799	-0.475799
$\alpha_C^C/\text{\AA}^{-2}$	-0.191945	-0.018958	-0.018958	-0.102989	-0.018958	-0.018958
$\alpha_{BB}^C/\text{\AA}^{-1}$	0.841101	-0.308327	-0.155382	-0.728090	-0.441608	0.136459
α_0^B	0.289789	1.867800	0.165656	0.274980	2.074430	0.702795
α_H^B	-0.009747	-1.091110	-0.316241	0.042571	-1.886850	-0.042457
α_C^B	1.323840	2.139090	-1.191640	-0.378518	4.616360	-1.145650
α_{BB}^B	0.046013	0.469322	0.557571	0.022000	-0.044138	-0.110016
D_{HH}	-0.040104	-0.002121	-0.002121	0.009888	-0.002121	-0.002121
D_{HC}	0.137949	-0.020134	-0.020134	-0.026061	-0.020134	-0.020134
$\delta_{BB}^H/\text{\AA}$	-0.179276	0.119968	-0.381256	0.018716	-0.008092	0.010861
δ_H^C	-0.001134	0.050000	0.050000	-0.027138	0.050000	0.050000
D_{CC}	0.024080	0.003973	0.003973	0.003405	0.003973	0.003973
$\delta_{BB}^C/\text{\AA}$	-0.053271	0.104576	0.201632	0.068520	0.116599	-0.033598
V_0/cm^{-1}	0	3600	3600	0	3600	3600
D_{HH}/cm^{-1}	41671.5	54287.8	54287.8	60039.8	54287.8	54287.8
D_{HC}/cm^{-1}	11344.8	3228.6	3228.6	-11482.3	3228.6	3228.6
$c/\text{cm}^{-1}\text{\AA}^{-1}$	114035.0	66573.4	66573.4	100870.0	66573.4	66573.4
$i/\text{cm}^{-1}\text{\AA}^{-1}$	11056.6	153.6	8272.9	10591.4	75.0	5341.3
E_0^R/cm^{-1}	248.1	-7386.5	-9076.4	0.0	-6961.1	0.0
E_C^B/cm^{-1}	362784.0	-62222.6	49633.0	5227.4	-46671.6	43236.5
E_{CC}^B/cm^{-1}	-486440.0	53941.5	-20208.9	-409647.0	29038.2	7901.8

TABLE II. Summary of the Fits of the Potential Surfaces.

Potential	Data	n	Number of Unknowns	----- Error of Fit -----		
				χ^2 (cm ⁻¹)	%	largest (cm ⁻¹)
$V_n^{[X]}(\mathbf{q})$	all	73	32	22	.60	157
$V_v^{[X]}(\Delta\mathbf{r})$	all	70	27	40	.78	207
$V_v^{[A]} = V_n^{[A]}$	linear	28	16	5	.33	122
$V_n^{[A(^2A')]}(\mathbf{q})$	bent	29	16	20	.56	284
$V_n^{[A(^2A'')]}(\mathbf{q})$	bent	33	16	24	.61	232
$V_v^{[A(^2A')]}(\Delta\mathbf{r})$	bent	29	11	25	.59	331
$V_v^{[A(^2A'')]}(\Delta\mathbf{r})$	bent	33	11	4	.25	147

lata points, the number of adjustable parameters n , the final value of χ^2 , the average absolute error as a percentage of the average energy, and the largest recorded error. More detail and the CASSCF data points used are available on request from the authors. Most of the data points are within 10000cm^{-1} of the minima of the potential surfaces, though there are some points on each surface in excess of 15000cm^{-1} energy. Geometries with CCH angles as low as 100° are included in this data. Both forms of the potential surface fit the data well. The distribution of the errors in the fits are random and there is little correlation between corresponding normal and valence co-ordinate surface errors. Typically the functions fit the data to a tolerance of 0.5%, with the greatest error observed for any one point being 331cm^{-1} .

All energies reported in Table I and elsewhere are with respect to the minimum energy of the X state which is calculated to be -76.2636 Hartrees. The calculated spacing between the minima of the X and A states, $V_0^{[A]}$, is 5835cm^{-1} , in contrast to pure SCF calculations which actually place the A state at a little lower energy than the X state. Experimental results¹⁵ place $V_0^{[A]}$ near 3600cm^{-1} in reasonable agreement with multi-reference singles plus double CI results.¹⁹ Apparently the CASSCF treatment with five active σ orbitals and two active π orbital provides a somewhat better description of the X state than of the A state. We have computed $V_0^{[A]}$ using CI wavefunctions (including all singles and doubles replacements from the Hartree-Fock reference) in both our DZP basis and an extended van Duijneveldt gaussian basis⁴³ ($[13s\ 7p\ 2d]$ contracted to $[7s\ 4p\ 2d]$). At the CI singles plus double level, $V_0^{[A]}$ is 2173cm^{-1} and 2462cm^{-1} for the DZP and extended bases, respectively. These energies increase substantially to 2882cm^{-1} and 3046cm^{-1} when a correction is applied for quadrupole excitations.⁴⁴ Hence, as more of the valence correlation energy is recovered, a larger proportion of the differential correlation is recovered as well. It is likely that a fully converged CI calculation will produce a $V_0^{[A]}$ in good agreement with the experimental observation of near 3600cm^{-1} , so we use this value in our calculations instead of 5835cm^{-1} .

From the valence co-ordinate potential $V_v^{[X]}(\Delta\mathbf{r})$ the dimensionless normal co-ordinates \mathbf{q} are deduced. These co-ordinates have the frequencies $\nu_1 = 3623\text{cm}^{-1}$, $\nu_2 = 486\text{cm}^{-1}$ and $\nu_3 = 1971\text{cm}^{-1}$, where $\nu_i = \omega_i/2\pi c$. Dimensionless normal co-ordinates are produced in the usual fashion by weighting the dimensioned normal co-ordinates by $(\hbar\omega_i)^{1/2}$. The direction and length of these co-ordinates are then obtained⁴⁵ from the eigenvectors of the matrix of the mass weighted second derivatives of $V_v^{[X]}(\Delta\mathbf{r})$, expressed in cartesian co-ordinates. This information is contained within the parameters $L_{HH} = 0.099548\text{\AA}$, $L_{HC} = 0.013497\text{\AA}$, $L_{CH} = -0.011555\text{\AA}$, $L_{CC} = 0.051046\text{\AA}$ and $L_{BB} = 0.288801$. All of the normal co-ordinate potentials are written in terms of these dimensionless normal co-ordinates. Note that as all of the potential constants are refitted to the data when $V_n^{[S]}(\mathbf{q})$ are generated, the normal co-ordinate potentials need not have the same vibration frequencies as $V_v^{[X]}(\Delta\mathbf{r})$.

C. Dipole and Transition Moments

Equation (2.6) requires the result of the dipole moment operating on the gaussian wave packet to be propagated on the excited potential surface. This can be propagated without further approximation^{26, 46} if μ can be expanded as a power series in the dimensionless normal co-ordinates \mathbf{q} . In principle, all terms in the expansion can be accommodated but at present only constant and linear terms are included in the spectral programs. When higher order terms are small in comparison to these terms (this does not apply to the CC stretch component of the X state dipole moment), their effect may be approximated by locally expanding μ as a linear function.

Vibrational transitions to levels with Σ^+ symmetry are polarized parallel (\parallel) to the molecular axis. The associated dipole moment, μ_{\parallel} , is an even function of the bend co-ordinates. Conversely, transitions to levels with Π symmetry are polarized perpendicular (\perp) to the molecular axis and the dipole moment μ_{\perp} is an odd function of the bend co-

TABLE III. Transition Moment and Dipole Moment Coefficients, in Debyes.

Constant	X	$A(^2A') \leftarrow X$	$A(^2A'') \leftarrow X$
μ_0	0.725579	0.549164	0.549164
μ_H	0.089610	0.008069	0.008069
μ_C	0.026924	-0.024602	-0.024602
μ_{HH}	-0.001546	-0.000791	-0.000791
μ_{HC}	0.007610	0.000451	0.000451
μ_{CC}	0.000474	-0.001439	-0.001439
μ_{VV}	0.014547	-0.032514	0.007478
μ_{HVV}	-0.002859	0	0
μ_{CVV}	0.023797	0	0
μ_{HHVV}	0.000146	0	0
μ_{HCVV}	0.001957	0	0
μ_{CCVV}	-0.001607	0	0
μ_{VVVV}	-0.002209	0.001615	0.000713
μ_V	0.168037	0.319952	
μ_{HV}	0.006908	0	
μ_{CV}	-0.030209	0	
μ_{HNV}	0.003773	0	
μ_{HCV}	-0.003326	0	
μ_{CCV}	0.000769	0	
μ_{VVV}	0.005092	0.000382	
μ_{HHNV}	0.000198	0	
μ_{HHCV}	-0.000189	0	
μ_{HCCV}	-0.000041	0	
μ_{CCCV}	0.000560	0	
μ_{HVVV}	0.001286	0	
μ_{CVVV}	0.000629	0	

C₂H X VIBRATIONAL ABSORPTION

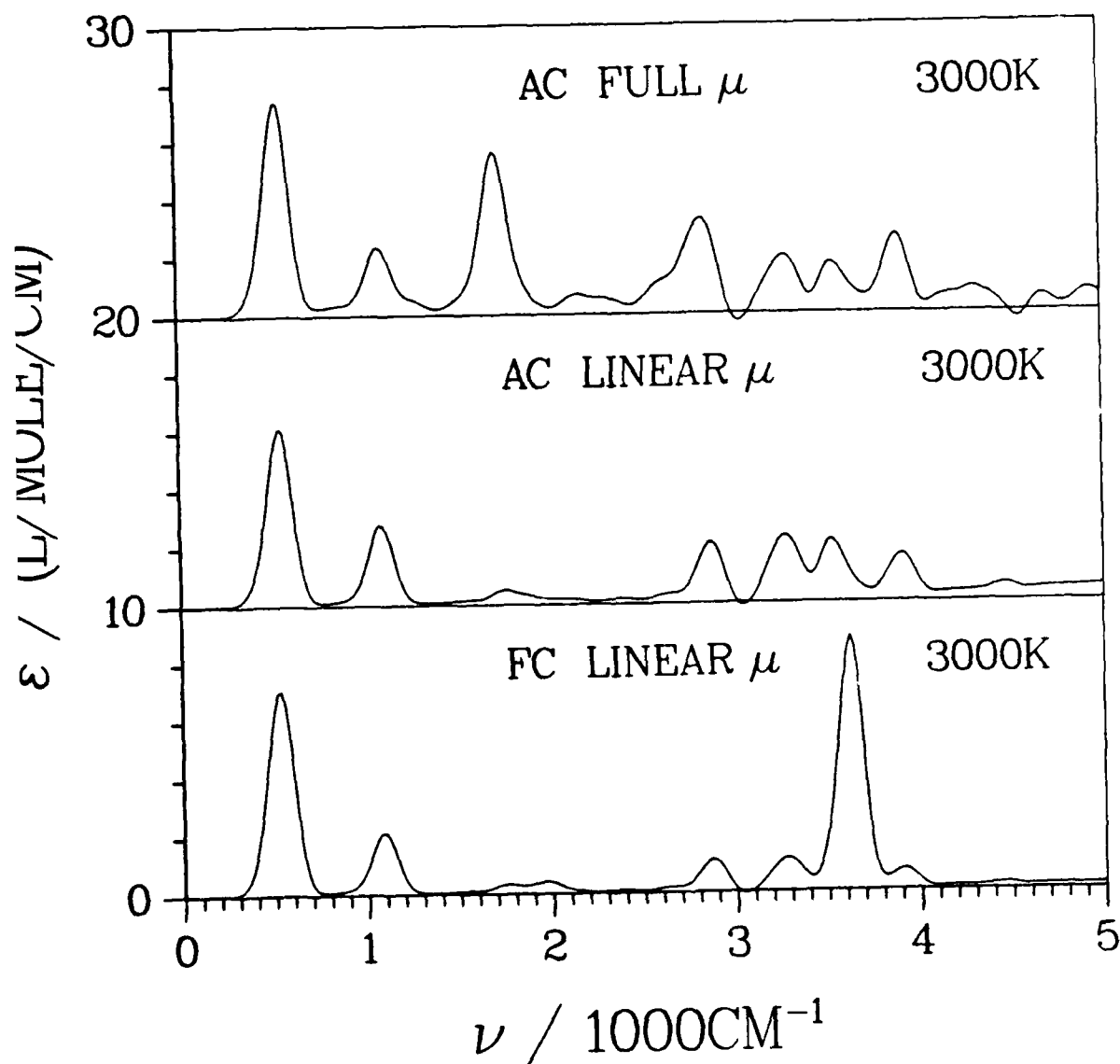


Figure 5. Vibrational Absorption Spectrum calculated using either the FC or AC methods and either the full dipole moment or only its linear components.

large number of vibrational states which contribute to the spectrum, in contrast to the previous room temperature calculation of the water molecule infrared and Raman spectra.⁵¹ We thus calculated the vibrational spectrum at 3000K using classical linear response theory,⁵² as formulated by Berens and Wilson.⁵³ In this approach the classical autocorrelation (AC) of the dipole moment is computed and Fourier transformed to give the infrared spectrum. At the harmonic level this approach gives the correct quantum intensities for the fundamental vibrations at non-zero temperature.⁵³ Non-linear components of the dipole moment are easily included in this calculation. It has the disadvantages, however, of incorrect detailed balance for overtone and combination bands, of an incorrect representation of the anharmonic coupling, and it can not be applied as $T \rightarrow 0$.

Figure 5 gives the spectrum calculated using both the wave packet (FC) and classical autocorrelation (AC) methods at 3000K. The results for the linear dipole are remarkably similar for seven of the eight observed bands, but the intensity profile of ν_1 is reduced by a factor of four in the AC calculation. These calculations have been repeated using a single harmonic oscillator and the results compared to exact quantum calculations.²⁶ The full quantum and AC results are almost identical and have an intensity of only 75% of the FC result. This discrepancy is due to the reduced temperature $kT/\hbar\omega$, which for this vibration is 0.6, in the intermediate region where the classical temperature approximation is least appropriate. This intensity is also three times larger than the intensity calculated using the AC technique on the full potential. In Figure 5, most of the CH stretch intensity is dispersed by the anharmonicity, appearing in both the combination and overtone bands and in the elevated base line. Such a dispersion is unrealistic and the FC calculation gives a better description of the overtone and combination band intensities.

Classical autocorrelation function calculations may also be performed using the full dipole moment profile, and the results are also given in Figure 5. The most striking feature of this spectrum is the five fold increase in intensity of the CC stretch, ν_3 . Crude time-independent calculations using harmonic potentials and only the μ_c and μ_{cbb} terms from the dipole moment expansion give results in excellent agreement with this result. The extra intensity arises from many hot bands which are not resolvable from each other at 60cm^{-1} resolution. High-resolution high-temperature spectra are expected to be very complicated.

B. Electronic Spectra

Calculated spectra over the temperature range 0-3000K are given in Figure 6 for the $A(2A'') \leftarrow X$ transition. The results are easily understood in terms of a standard eigenstate picture. At 0K we see a typical Frank-Condon progression based on the an allowed (perpendicular) origin at 3400cm^{-1} . This frequency is less than the energy difference between the potential minima (3600cm^{-1}) because of the zero point energy decrease in the $A(2A'')$ state. Normally a frozen gaussian calculation would not correctly detect this change (as a thawed gaussian calculation would) and here it has been added in an *ad hoc* fashion before Fourier transforming. In reduced units the $A(2A'')$ potential minimum is displaced by $q_1 = -0.15$ and $q_3 = 1.58$ from the X potential minimum. The progression in ν_3 thus has some length and the line spacing seen in the spectra is 1620cm^{-1} , very close to the harmonic A state CC stretch frequency of 1655cm^{-1} . Just to the blue of the third strong peak is the first line of a progression corresponding to an excitation of one quanta in the CH stretch ν_1 . Most of this intensity comes from the 1:2 Fermi resonance between the stretching motions. The tiny peaks at 1900cm^{-1} and 3800cm^{-1} are artifacts due to the approximate propagation methods used.

As the temperature is raised to 1000K, hot bands in the CC stretch vibration appear. A transition from vibrational level i to vibrational level j of the n th vibration is labeled as $i \rightarrow j n$. The origin of this hot band is thus labeled as 0_3 , and the progression based upon it is 350cm^{-1} to the red of the "cold" lines based upon the origin O ($0_1^0 0_2^0 0_3$).

C₂H X VIBRATIONAL ABSORPTION

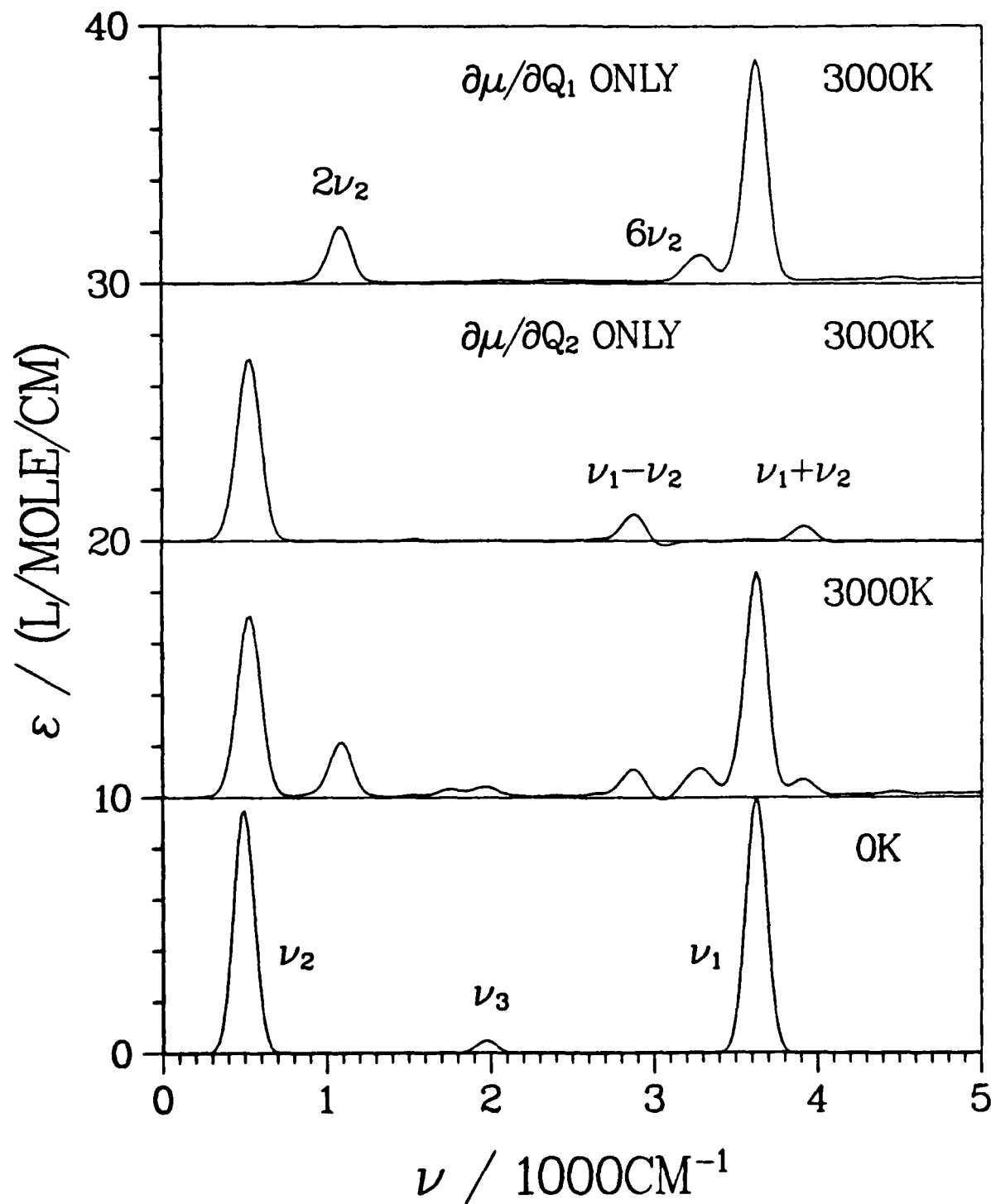


Figure 4. Vibrational Absorption Spectrum calculated using the F' method and either all or part of the linear dipole moment derivative terms.

It is also possible to approximate the center of the absorption band by examining what difference contours lie above the most probable regions. At $T = 0$ this gap is 5630cm^{-1} . At 3000K the most probable region for the $A(^2A'') \leftarrow X$ transition lies on similar energy contours and so the absorption band is expected to broaden but not shift in band center. Due to the repulsion of the $A(^2A')$ surface, the energy gap in the probable 140° - 160° range of bond angle is $3\text{-}4000\text{cm}^{-1}$ larger than it is at the equilibrium configuration. The $A(^2A') \leftarrow X$ absorption band is thus expected to be significantly blue shifted at 3000K. This line of argument can be formalized and a simple, almost classical, algorithm developed for the determination of the absorption band contour.⁴⁸

V. CALCULATED SPECTRA

A. Vibrational Spectra of the X State

Figure 4 shows the infrared vibrational spectra of the X state of C_2H calculated using the Frozen gaussian - Classical temperature (FC) approximations to wave packet dynamics. Only the linear components of dipole moment function are used in these calculations. The spectrum at 0K is precisely the spectrum which would be obtained using harmonic approximations and time independent quantum mechanics. Here the intensities are proportional to the square of the dipole moment derivatives. There is a large difference between the calculated and observed intensities. From the low temperature spectra of Jacox,¹³ the CH stretch ν_1 is seen to be about three times as intense as the CC stretch ν_3 , while Figure 4 shows ν_1 to be about 20 times more intense. Also the bend absorption ν_2 is calculated to be quite strong, whereas this vibration has never been directly observed. The approach taken here adequately describes the low temperature infrared intensities of many molecules, including ozone,³⁴ but seems inappropriate for C_2H .

The discrepancy between the intensity ratios for ν_1 and ν_3 is due largely to the neglect of non-linear and anharmonic terms. In principle, the electrical non-linearity may be included directly into the FC calculations,²⁶ but it is much more difficult to include the effects of mechanical anharmonicity.^{46,49} Here, we choose to perform an expensive time-independent calculation, diagonalizing the vibrational hamiltonian matrix to account for the mechanical anharmonicity, while evaluating all of the dipole moment matrix elements to account for the electrical non-linearity. In Table VI, all absorption bands with significant intensity are listed. Now ν_1 is only five times more intense than ν_3 , in much better agreement with experiment. The increased intensity in ν_3 comes largely from the non-linear μ_{CBB} term in the dipole moment function.

When the molecule is heated to 3000K, many overtones appear due to the increased sampling of the mechanical anharmonicity. The calculated absorption band shown in Figure 4 is quite complicated but may be assigned by performing calculations with some components of the dipole profile removed. With only the perpendicularly polarized intensity present (only $\partial\mu/\partial q_2$ non zero) three bands result. These all must have odd quanta in the bend mode ν_2 . At low temperatures the two high frequency bands are symmetrically distributed around ν_1 and are clearly $\nu_1 + \nu_2$ and $\nu_1 - \nu_2$. As the temperature increases both bands move to lower frequency and their symmetric location about ν_1 is lost, as shown in Figure 4. Also shown in Figure 4 is the intensity pattern when only $\partial\mu/\partial q_1$ is non zero. Three bands again result, and these must all have even quanta in the bend quantum number. They are assigned as the CH stretch fundamental ν_1 and the overtones $2\nu_2$ and $6\nu_2$. As the 3:1 Fermi resonance is strong compared to the 6:1 resonance,⁵⁰ $2\nu_2$ is expected to be more intense than $6\nu_2$, as observed. $4\nu_2$ is very weak as it is both poorly resonant (4:1) and widely separated in energy.

The previous calculations are performed using several approximations. One way to test for their applicability is to calculate the spectra using an independent technique. Currently, it is not feasible to use time-independent methods at 3000K due to the very

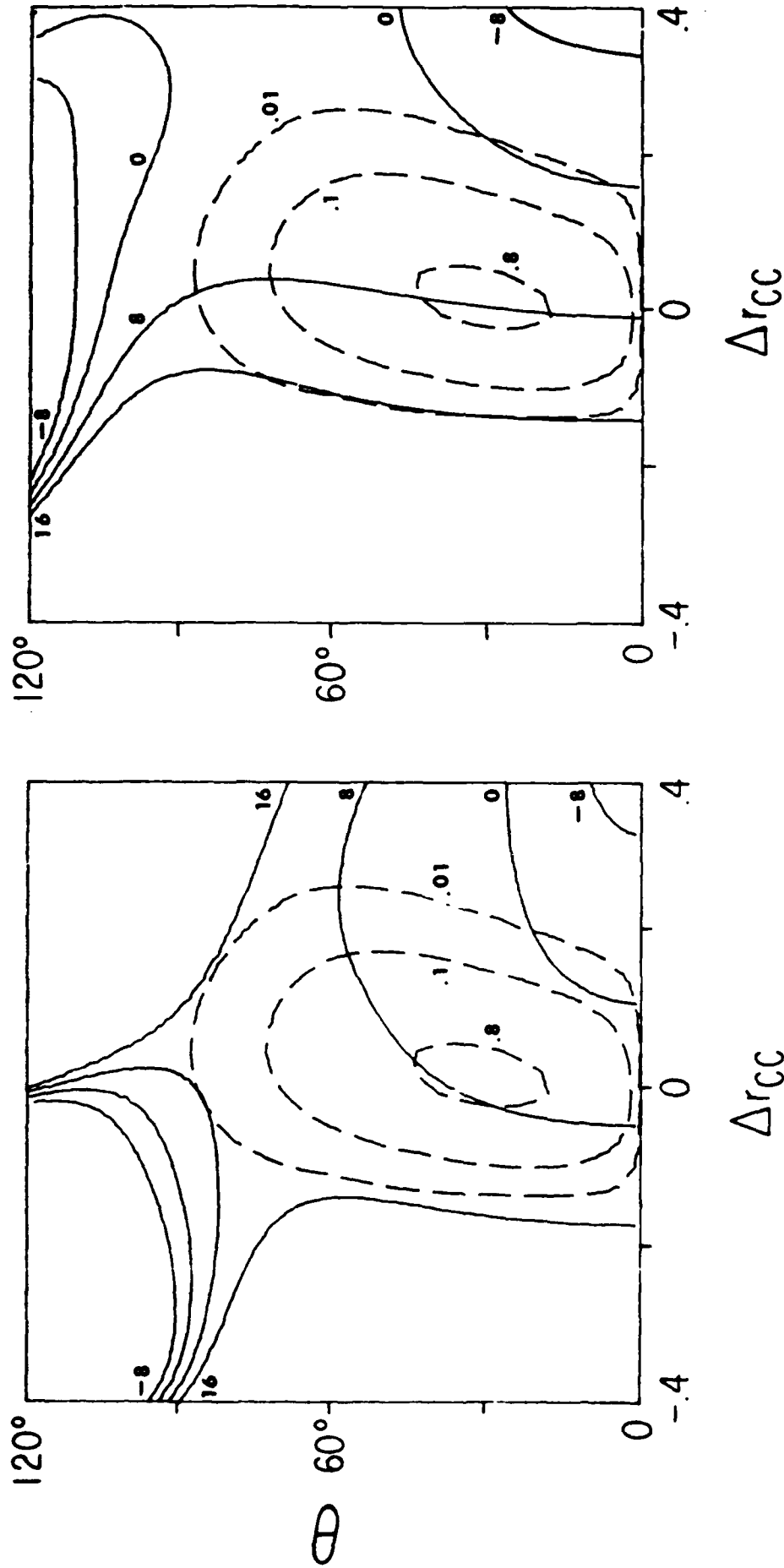


Figure 3. Surface Crossing Effects. — Potential difference contours in 1000cm^{-1} between the $V_j^X(\Delta r)$ potential and either the $V_j^A(\Delta r)$ potential (left) or the $V_j^B(\Delta r)$ potential (right) at $\Delta r_{CH}=0$. ---- relative probability of being at this configuration on the ground state at 3000K.

the normal co-ordinate potential, attributable the better fit near the C_{2v} region.

C. Bond Angle Distribution at High Temperature

The most striking features of equations (4.4)-(4.5) is the multiplicative factor of $\sin\theta$ in equation (4.5). Classically, a molecule with a linear equilibrium geometry has, at non-zero temperature, zero probability of actually being linear, see Figure 2. This result can be understood in terms that linear molecules have two degenerate bending components. It is quite likely that any one of these components be within $d\theta$ of θ but of vanishing probability that both components will simultaneously be within this range, as is needed for the molecule to be truly linear. Dynamical approaches can also be used to explain this result. Suppose that the molecule is bent and given a random velocity in both directions perpendicular to the molecular axis. This velocity will have a component in the plane of the bent molecule and a component perpendicular to it. The perpendicular component produces angular momentum around the molecular axis which must be conserved as the molecule moves. If the molecule is to become linear then the corresponding moment of inertia would vanish and so the rotational kinetic energy would become infinite! Motion on the true four dimensional surface can be viewed as motion on a reduced three dimensional surface with a bend potential modified to include this centrifugal barrier which forces the trajectory to stay out of the linear region.

Quantum mechanics modifies this purely classical picture primarily by broadening the distributions due to zero point motion. The width of the ground state wave function is about 15° and so the classical probability functions are only slightly broadened. These effects are included in the subsequent spectral calculations: indeed, wave packet dynamics can be used to construct the quantum probability functions, if desired. For stiff molecules like HCN at reasonable temperatures, the peak in this probability function is close to 180° and the molecule can be treated as being truly linear. On the other hand, for floppy molecules such as C_2H at high temperatures, there are large displacements from linearity. The classical average angle for C_2H is 145° at 3000K and as a result it should not be regarded as a linear molecule at this temperature. This effect dominates the $A(^2A') \leftarrow X$ spectrum.

D. The Intersection Region of the Surfaces

In the linear configuration the X and A surfaces cross when $r_{CC} = 1.348\text{\AA}$ at an energy of 3870cm^{-1} . Shih, Peyerimhoff and Buenker¹⁹ obtained similar results. This crossing is very close to the minimum energy configuration of the excited state and its ramifications are expected^{20, 47} to be severe on low temperature spectra. When the molecule bends, the crossing of the X and $A(^2A')$ surfaces becomes sharply avoided. This is shown in Figure 3, where the vertical excitation energies from the X surface to both the $A(^2A')$ and $A(^2A'')$ surfaces are plotted as contours at $\Delta r_{CH} = 0$ ($r_{CH} = 1.056\text{\AA}$). The value of Δr_{CC} at the crossing of the X and $A(^2A'')$ states is a relatively insensitive function of bond angle, however, the crossing of the X and $A(^2A')$ states is quite sensitive to the bond angle. Because of the rapid increase in energy of the $A(^2A')$ state as the molecule bends, the intersection point moves to very large CC distances. Note that the potential contours are somewhat insensitive to the value of Δr_{CH} at which they are evaluated.

Also plotted in Figure 3 are contours of equal probability for the $V_v^{(X)}(\Delta r)$ potential at 3000K. These contours are centered around a bond angle of 145° , as noted previously. The overlap of this set of contours with the previous set demonstrates that the intersection region is not significantly populated at 3000K. Not only is it improbable to get direct Franck-Condon transitions into this region, but also the centrifugal barrier prevents the excited state trajectories from entering it. Thus, the non-adiabatic effects are reduced^{20, 47} as the temperature increases.

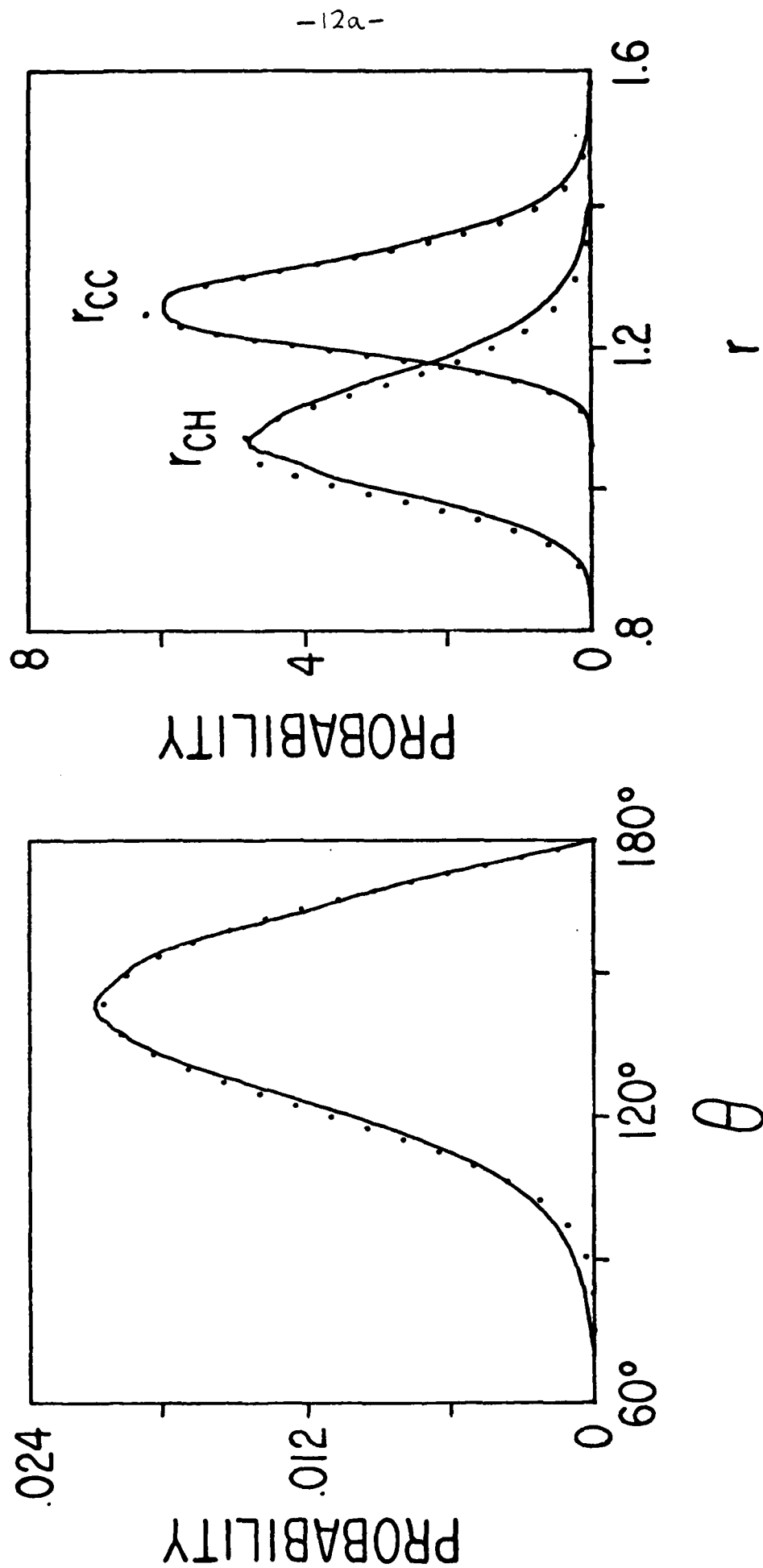


Figure 2. Bond Length and Angle Probabilities at 3000K. — evaluated from $V_n^{|X|}(q)$, evaluated from $V_n^{|X|}(\Delta r)$.

should not be run on these surfaces at energies near either the saddle point energies or end-over-end rotation energies. Figure 2 is used to demonstrate *a posteriori* that such trajectories are not common at a temperature of 3000K. It shows the classical ensemble averaged values of the bond lengths and angles at 3000K for both the $V_v^{[X]}(\Delta\mathbf{r})$ and $V_n^{[X]}(\mathbf{q})$ potentials, and these show little penetration into the poorly represented regions. Expressions for these average values can be obtained by considering the partition function, which for the normal co-ordinate potential is

$$Q_n = \int_{-\infty}^{\infty} dq_1 dq_{2a} dq_{2b} dq_3 e^{-\beta V_n^{[X]}(\mathbf{q})} . \quad (4.1)$$

Noting that $V_n^{[S]}(\mathbf{q})$ are only functions of $q_2 = (q_{2a}^2 + q_{2b}^2)^{1/2}$, we can introduce the "polar" co-ordinates q_2 and ϕ , as is done in equation (3.2), simplifying the partition function to

$$Q_n = 2\pi \int_{-\infty}^{\infty} dq_1 dq_3 \int_0^{\infty} dq_2 q_2 e^{-\beta V_n^{[X]}(\mathbf{q})} . \quad (4.2)$$

A similar result applies to the partition function expression written in terms of valence coordinates, resulting in

$$Q_v = \int_0^{\infty} d\tau_{CH} d\tau_{CC} \int_0^{\pi} d\theta \sin\theta e^{-\beta V_v^{[X]}(\Delta\mathbf{r})} . \quad (4.3)$$

Here, the $\sin\theta$ term arises from the transformation from cartesian to valence co-ordinates, equation (3.1). The probabilities of being within $d\tau_{CH}$ of τ_{CH} , $d\tau_{CC}$ of τ_{CC} and $d\theta$ of θ are given by

$$\int_0^{\infty} d\tau_{CC} \int_0^{\pi} d\theta \sin\theta e^{-\beta V_v^{[X]}(\Delta\mathbf{r})} , \quad (4.4)$$

$$\int_0^{\infty} d\tau_{CH} \int_0^{\pi} d\theta \sin\theta e^{-\beta V_v^{[X]}(\Delta\mathbf{r})} \quad (4.5)$$

and

$$\sin\theta \int_0^{\infty} d\tau_{CH} d\tau_{CC} e^{-\beta V_v^{[X]}(\Delta\mathbf{r})} , \quad (4.5)$$

respectively. Parallel equations exist for these probabilities written in terms of normal coordinates.

In Figure 2 the bond length distributions are well within the reliability range of the fitted X potential functions. Unfortunately the angle distribution has a slight tail to large angles, into the end-over-end hydrogen rotation region. Trajectories which start in this region of the potential are not run in the subsequent spectral calculations. This is not a significant error in the calculation. It is clear that these potential surfaces are inappropriate at temperatures significantly higher than 3000K for which end-over-end rotation needs to be included explicitly.

A method for estimating the reliability of the A surfaces is to take the most probable regions on the X state and look at the excited state surfaces, not only in this region, but in all regions energetically accessible to excited state trajectories starting with these ground state geometries. The excited state data points are chosen to span this entire region, and about 1% of all the trajectories which were run were found in poorly represented regions.

The probability distribution functions for both the normal and valence co-ordinate potentials are given in Figure 2 as a final check on the accuracy of the functions. Clearly, both potentials are very similar. The major differences in the probability functions are first, a shift of 0.015Å in the τ_{CH} probability, attributable to inadequacies in the bend-CH stretch potential (see Figure 1); and second, the longer tail to low angle on

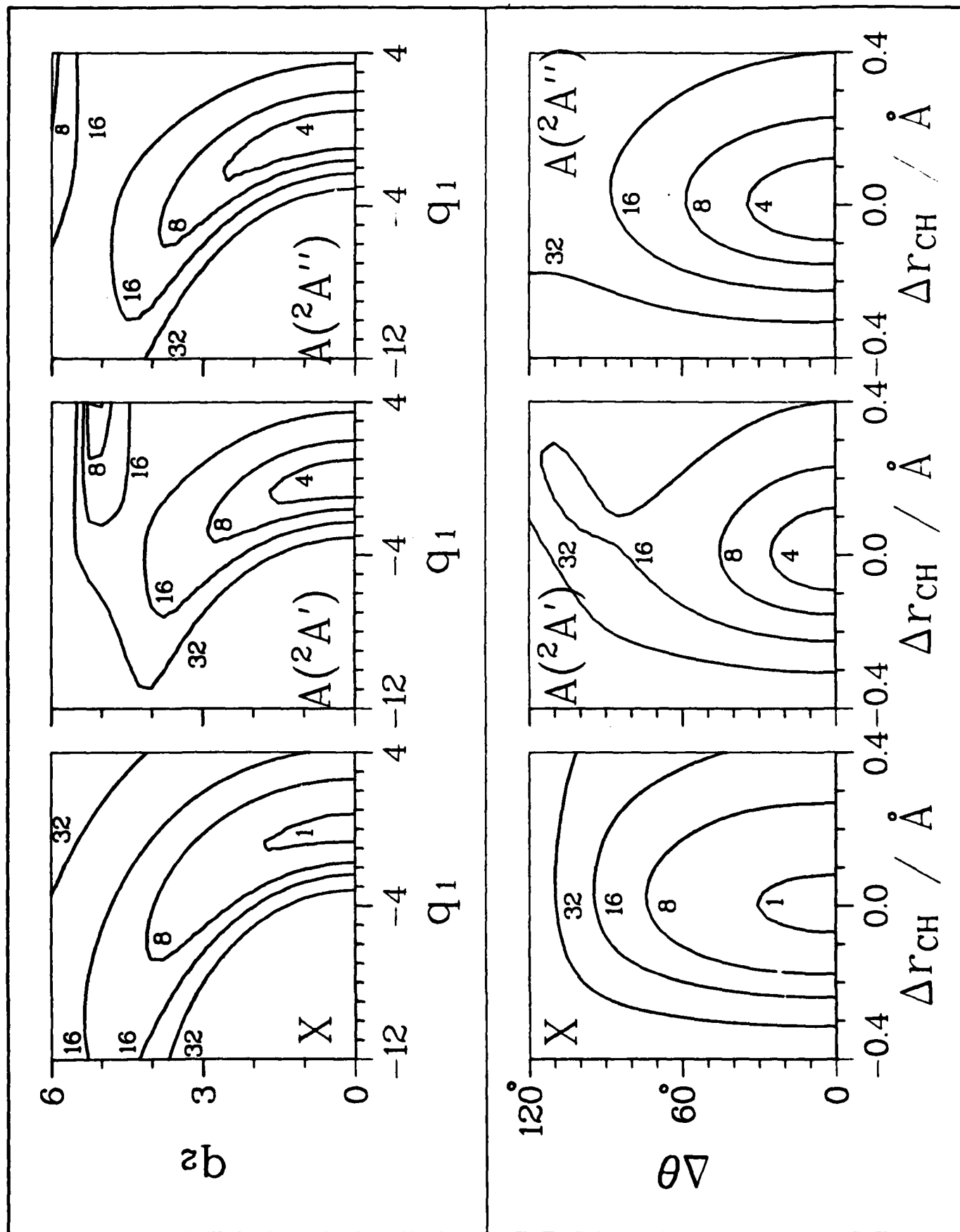


Figure 1. Potential Contours in 1000cm^{-1} above each states own minimum. Top panel gives normal co-ordinate contours at $q_2=0$. Bottom panel gives valence co-ordinate contours at $\Delta r_{CH}=0$.

The calculated X state CH stretch harmonic vibrational frequencies are nearly the same, 3645cm^{-1} and 3623cm^{-1} , for $V_v^{[X]}(\Delta\mathbf{r})$ and $V_n^{[X]}(\mathbf{q})$, respectively. When anharmonicity is included the frequency for $V_n^{[X]}(\mathbf{q})$ decreases to 3484cm^{-1} , slightly less than the value of 3612cm^{-1} observed¹³ by Jacox. In the A state the CH stretching frequency is slightly reduced. The CC harmonic stretch frequency is calculated to be near 1975cm^{-1} in the ground state. Anharmonic corrections reduce this to 1900cm^{-1} , not far from the observed¹⁸ value of 1848cm^{-1} . In the A state the corresponding harmonic frequency is 1655cm^{-1} , and anharmonic corrections will likely bring this very close to the observed¹² value of $1560 \pm 40\text{cm}^{-1}$. For the bending vibration the calculated harmonic frequencies are around 494cm^{-1} ; anharmonic corrections reduce this to 470cm^{-1} . This frequency has never been directly observed. Carrick, Merer and Curl¹⁵ deduced, by analyzing the *l*-type doubling in their electronic spectra, that it lies in the range $390\text{--}475\text{cm}^{-1}$; arguing that this range is conservative, they then went on to postulate that the frequency is actually 375cm^{-1} . Clearly, further experimental studies need to be performed in order to measure this frequency more reliably. In the excited $A(^2A')$ surface this frequency decreases slightly but it more than doubles in the excited $A(^2A')$ surface. This is brought about by the repulsion between the lower $X(^2A')$ and upper $A(^2A')$ surfaces, and has a very important effect on high temperature spectra.

B. Useful Range of the Potentials

Figure 1 contains contour plots of sections cut through the surfaces and indicates the magnitude of the anharmonicity of C_2H . The top three inserts in this figure display $V_n^{[S]}(\mathbf{q})$ cut through the section $q_3 = 0$, while the lower inserts display $V_v^{[S]}(\Delta\mathbf{r})$ cut through the section $\Delta r_{\text{CC}} = 0$. Here the contours, in 1000cm^{-1} , are given with reference to the minima of the respective potential surfaces *S*. As the $A(^2\Pi)$ surface is displaced in the CC stretch variable the lowest energy in both of the A sections is 2027cm^{-1} above the A state potential minimum. From the shape of the contours we see both the intrinsic advantage of writing the potential in valence co-ordinates and the effectiveness of the non-linear transformation, equations (3.20)-(3.22).

These plots extend in geometry far beyond the region of the potential that is fitted to the *ab initio* data (most of the data points have energies $< 10000\text{cm}^{-1}$, very few have energies $> 16000\text{cm}^{-1}$). In the fitted regions the potentials fit the data well. Spurious saddle points exist outside this region, however. Consequently these surfaces are not suitable for extrapolation purposes. Included in Table V are the geometries and energies of the lowest found saddle point for each potential surface.

The valence co-ordinate potentials are slightly less susceptible to low lying saddle points. In some respects this is a disadvantage as the normal co-ordinate potentials represent better the turn-over of the bend potential which occurs as the C_{2v} geometry is approached. From Table V the valence potential predicts that a saddle point lies on the X surface at $r_{\text{CH}} = 1.33\text{\AA}$, $r_{\text{CC}} = 1.34\text{\AA}$, $\theta = 57^\circ$ and an energy of 14789cm^{-1} . As the largest angle used in the CASSCF data is 100° , this point represents a considerable extrapolation. Subsequent to the fitting of the potentials, more CASSCF calculations have been performed and the C_{2v} transition state for end-over-end hydrogen rotation calculated to be at $r_{\text{CH}} = 1.28\text{\AA}$, $r_{\text{CC}} = 1.29\text{\AA}$, $\theta = 63^\circ$ and an energy of 14509cm^{-1} . As the CASSCF energy increases quite slowly when all bonds are simultaneously extended, the accuracy of the extrapolation of the normal co-ordinate potential is quite remarkable. On the other hand the valence co-ordinate potentials tend to climb rapidly at small θ , showing no sign of turning over. If greater accuracy is needed, then a potential written in terms of the sine of the angle between the CC bond vector and the vector joining the hydrogen atom to the mid-point of the CC bond vector should be used. Such a function would possess the correct angle boundary conditions.

At moderate to high energy the surfaces are quite ergodic: a trajectory will quickly sample most of phase space that is energetically accessible to it. Thus trajectories

TABLE VI. Vibrational Absorption Frequencies and Intensities from the X state Normal Co-ordinate Porential.

Mode	Component	Frequency (cm ⁻¹)	Relative Intensity
ν_2	Π	470	1.
$2\nu_2$	Σ^+	980	0.02
ν_3	Σ^+	1900	0.17
$\nu_2 + \nu_3$	Π	2326	0.07
$2\nu_2 + \nu_3$	Σ^+	2857	0.03
ν_1	Σ^+	3484	0.94
$2\nu_3$	Σ^+	3778	0.001
$\nu_1 + \nu_3$	Π	3940	0.06
$\nu_1 + \nu_2$	Σ^+	5380	0.01
$2\nu_1$	Σ^+	6855	0.02

TABLE V. Properties of the Potentials.

	$V_n^{[X]}(\mathbf{q})$	$V_n^{[A(^2A')]}(\mathbf{q})$	$V_n^{[A(^2A'')]}(\mathbf{q})$	$V_v^{[X]}(\Delta\mathbf{r})$	$V_v^{[A(^2A')]}(\Delta\mathbf{r})$	$V_v^{[A(^2A'')]}(\Delta\mathbf{r})$
at equilibrium geometry						
ν_1/cm^{-1}	3645	3589	3589	3623	3589	3589
ν_2/cm^{-1}	504	1056	483	486	1075	545
ν_3/cm^{-1}	1976	1655	1655	1971	1655	1655
at lowest saddle point						
V/cm^{-1}	14789	20596	19241	57478	19375	18693
$r_{CH}/\text{\AA}$	1.330	1.406	1.504	19.667	1.143	1.143
$r_{CC}/\text{\AA}$	1.340	1.260	1.414	1.714	1.323	1.323
θ/deg	57	117	108	180	123	57

ordinates. The functional forms used to represent these components are

$$\mu_e = \mu_0 + \mu_H q_1 + \mu_C q_3 + \mu_{HH} q_1^2 + \mu_{HC} q_1 q_3 + \mu_{CC} q_3^2 + \mu_{BB} q_2^2 + \mu_{HBB} q_1 q_2^2 + \mu_{CBB} q_3 q_2^2 + \mu_{HHBB} q_1^2 q_2^2 + \mu_{HCB} q_1 q_3 q_2^2 + \mu_{CCBB} q_3^2 q_2^2 + \mu_{BBBB} q_2^4 \quad (3.20)$$

and

$$\mu_o = q_2 (\mu_B + \mu_{HB} q_1 + \mu_{CB} q_3 + \mu_{HHB} q_1^2 + \mu_{HCB} q_1 q_3 + \mu_{CCB} q_3^2 + \mu_{BBB} q_2^2 + \mu_{HHHB} q_1^3 + \mu_{HHC} q_1^2 q_3 + \mu_{HCCB} q_1 q_3^2 + \mu_{CCCB} q_3^3 + \mu_{HBBB} q_1 q_2^2 + \mu_{CBBB} q_3 q_2^2) \quad (3.21)$$

The electronic transition $A(^2\Pi) \leftarrow X(^2\Sigma^+)$ has different symmetry properties. It is perpendicularly polarized: μ_e is used to represent these components. When the molecule bends, the in-plane component of the transition moment is associated with the $A(^2A') \leftarrow X$ transition and the out-of-plane component is associated with the $A(^2A'') \leftarrow X$ transition. Bend displacements also introduce some parallel-polarized vibronic intensity: μ_o is used to represent this component of the transition moment. This intensity is associated with the $A(^2A') \leftarrow X$ transition only.

Minimization of the root mean square error

$$E_{rms} = \left[\frac{1}{n} \sum_n (\mu_{CASSCF} - \mu_{FIT})^2 \right]^{1/2} \quad (3.22)$$

is the condition used to determine the parameters in these expansions. As the number of *ab initio* data points for the transition moments is quite small, some of the cross terms in these expansions are constrained to be zero. Different refinements are performed for both of the odd and even functions and for both the pure-stretch and bend-containing subsets of the functions. The calculated constants are given in Table III, and a summary of the fits is given in Table IV including the error term E_{rms} , the number of free parameters, and the number of data points. More details are available from the authors. Note that the bending X dipole moment functions fit the data points with bond angles $< 145^\circ$ very well: most of the errors reported in Table IV arise from the data points with bond angle in the range 100° to 145° .

These expansions in terms of the dimensionless normal co-ordinates converge quickly. The only high-order constants that are appreciable are μ_{BB} , μ_{CBB} and μ_{CB} . Similar fits to the *ab initio* data have been attempted by expanding in powers of the valence co-ordinates Δr , $\Delta \alpha$, etc., are not reported here as the fits are unstable, having large high order terms. Apparently the normal co-ordinates provide a better description of the dipole moment surface than do the valence co-ordinates.

IV. PROPERTIES OF THE POTENTIALS

A. Vibration Frequencies

Table V gives details of a harmonic analysis of the potential minima. All minima have linear geometries and their bond lengths may be obtained directly from the parameters given in Table I. To get an indication of the effects of anharmonicity, the vibrational hamiltonian matrix for the $V_n^{[X]}(q)$ potential is constructed in the normal co-ordinate basis, truncated at states with more than a total of eight quanta (a grand total of 495 states are included), and then diagonalized. A product form Gauss-Hermite quadrature is used to evaluate the matrix elements. Some of the eigenvalues are given in Table VI, relative to the zero point energy which is found to be 3240cm^{-1} . The one and two quanta levels are believed to be converged to $\pm 10\text{cm}^{-1}$ and $\pm 40\text{cm}^{-1}$, respectively: note, however, that no rotational corrections²⁷ are included in these calculations.

TABLE IV. Summary of the Fits of the Dipole and Transition Moments.

Moment	Form	Polarisation	Data	n	Number of Unknowns	Error of Fit E_{rms} (Debyes)
X	μ_e		linear	33	6	.0006
X	μ_e		bent	33	7	.0589
X	μ_o	\perp	bent	33	13	.0110
A \leftarrow X	μ_e	\perp	linear	16	6	.0016
A($^2A'$) \leftarrow X	μ_e	\perp	bent	4	2	.0073
A($^2A'$) \leftarrow X	μ_o		bent	4	2	.0500
A($^2A''$) \leftarrow X	μ_e	\perp	bent	4	2	.9036

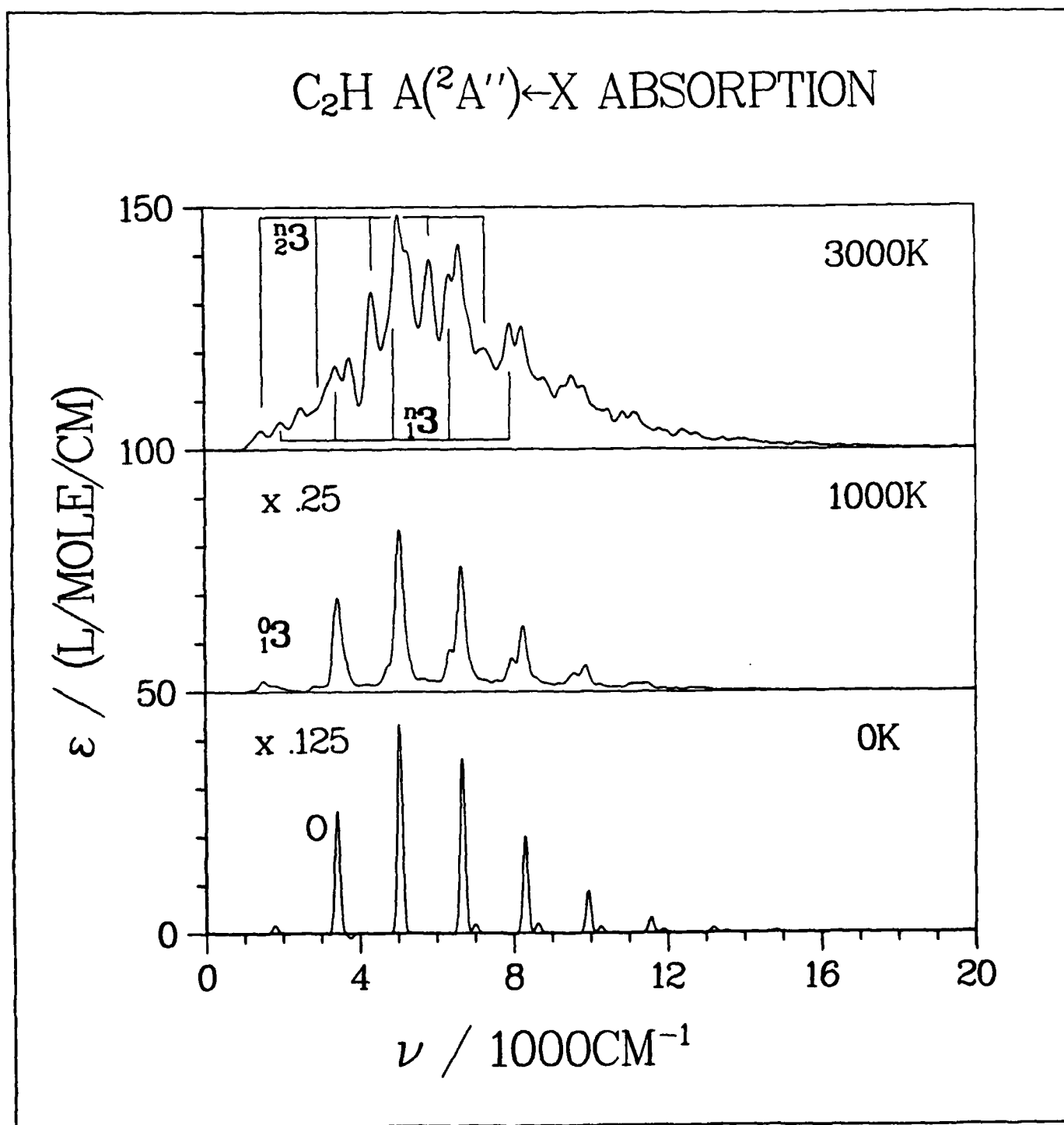


Figure 6. Electronic $A(^2A'') \leftarrow X$ Absorption Spectrum.

Each line is broadened by unresolved hot bands $1_2^0 3$ expected slightly to the red of the main $0_2^0 3$ lines. There is also a small intrinsic broadening due to the use of the frozen gaussian approximation for propagation on an anharmonic potential surface.²⁶ At 3000K the spectrum contains the cold lines $0_2^0 3$ as well as two hot band progressions $1_2^1 3$ and $2_2^1 3$. Lines are drawn on Figure 5 to highlight these hot band progressions. The 3000K spectrum is broadened due to the large number of lines present, and only partial structure remains at 60cm^{-1} resolution.

The calculated spectra for the $A(^2A') \leftarrow X$ transition, Figure 7, are much more difficult to interpret. There is both a perpendicular band based upon the allowed origin O and also a parallel band based upon the vibronic origin 0_2^0 . The perpendicular band at 0K is almost identical to the perpendicular band for the $A(^2A'') \leftarrow X$ transition except that the zero point correction shifts the origin up to 3960cm^{-1} . At 1000K the perpendicular spectra of the two states are quite different. Hot bands $1_2^1 2$ are spaced progressively at 550cm^{-1} to the blue of all of the 0K lines and fill the gaps between the $0_2^0 3$ progression. The intensities of these lines are highly non-Boltzmann with both $1_2^1 2$ and $2_2^1 2$ being stronger than $0_2^0 2$. This enhancement comes from the high anharmonicity of the excited state bend. The $A(^2A')$ potential decreases markedly in curvature at large angle, thus increasing the overlap between its wave functions and the ground state wave functions.

There are problems with the frozen gaussian approximation which even at 0K have more profound effects than just missing the changes in the zero point levels. Even though there is no displacement in the bend co-ordinate between the minimum energy configuration of the ground and excited states, Frank-Condon factors linking levels like $0_2^0 2$ can be significant. This is due to the large frequency change between the ground and excited state bending vibrations. Thus a second progression, based upon the origin O and spaced at 2100cm^{-1} , should be present. Thawed gaussians know about the frequency change and trial calculations performed using them indicate that $0_2^0 2$ is about five times weaker than $0_2^0 2$. Thus the error in using frozen gaussians is not great. At higher temperatures there is motion in the bend co-ordinate and thus the calculation knows about the frequency change. In the 1000K spectrum the shoulder at 5960cm^{-1} to the left of the fifth strong band is $0_2^0 2$ and a progression in ν_3 can be seen based upon this line. The large number of lines resulting at high energy can not be distinguished at 60cm^{-1} resolution.

Results for the forbidden parallel band, also given in Figure 7, show essentially the same features. The problem with the frozen gaussian approximation at 0K in not detecting the true excited state bend frequency now results in the vibronic origin $0_2^0 2$ being seen 550cm^{-1} to the red of where it should be. Again at 1000K the lines move to their correct location.

Figure 8 gives the total $A \leftarrow X$ spectra at 0K, 1000K and 3000K as a sum of the individual $A(^2A') \leftarrow X$ and $A(^2A'') \leftarrow X$ spectra. The doublets in the 0K spectra arise due to the difference in the zero point energies of the two A state components. Inadequacies in this spectrum have been discussed previously: the red shift of 550cm^{-1} in the parallel transitions and the absence of the weak $0_2^0 2$ progression. At 1000K the large number of new lines which appear washes out the structure at high energy. This continues as the temperature rises and at 3000K very little structure remains at 60cm^{-1} resolution. There is a large blue shift in the intensity distribution at high temperatures due to the repulsive nature of the $A(^2A')$ surface combined with the large value of the average ground state bend angle. The maximum intensity in the spectrum is shifted to 9500cm^{-1} . Some indication of a two band structure is present in the spectra with the $A(^2A'') \leftarrow X$ band appearing as a shoulder 4000cm^{-1} to the red of the intense $A(^2A') \leftarrow X$ band.

C_2H $A(^2A') \leftarrow X$ ABSORPTION

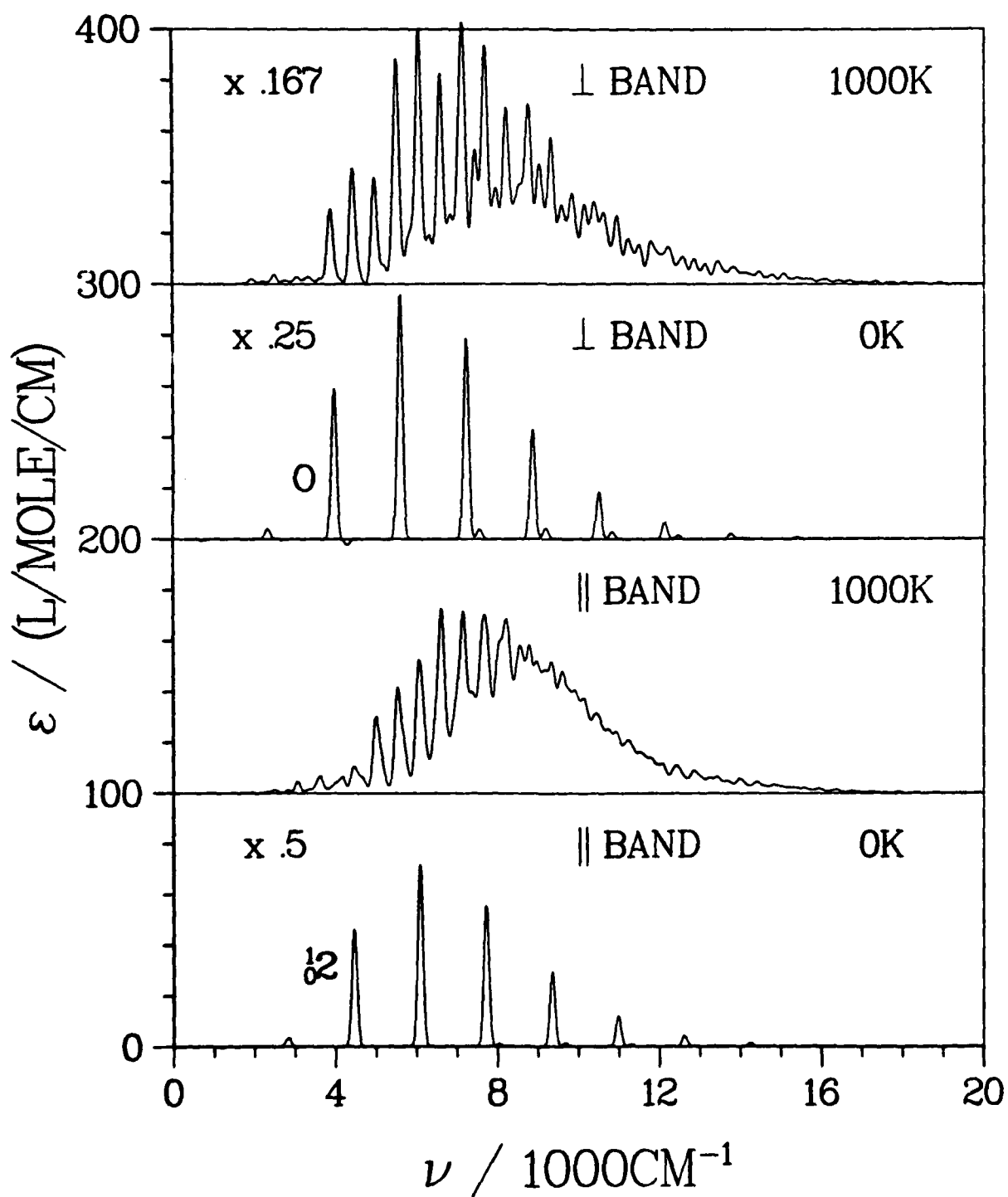


Figure 7. Electronic $A(^2A') \leftarrow X$ Absorption Spectrum.

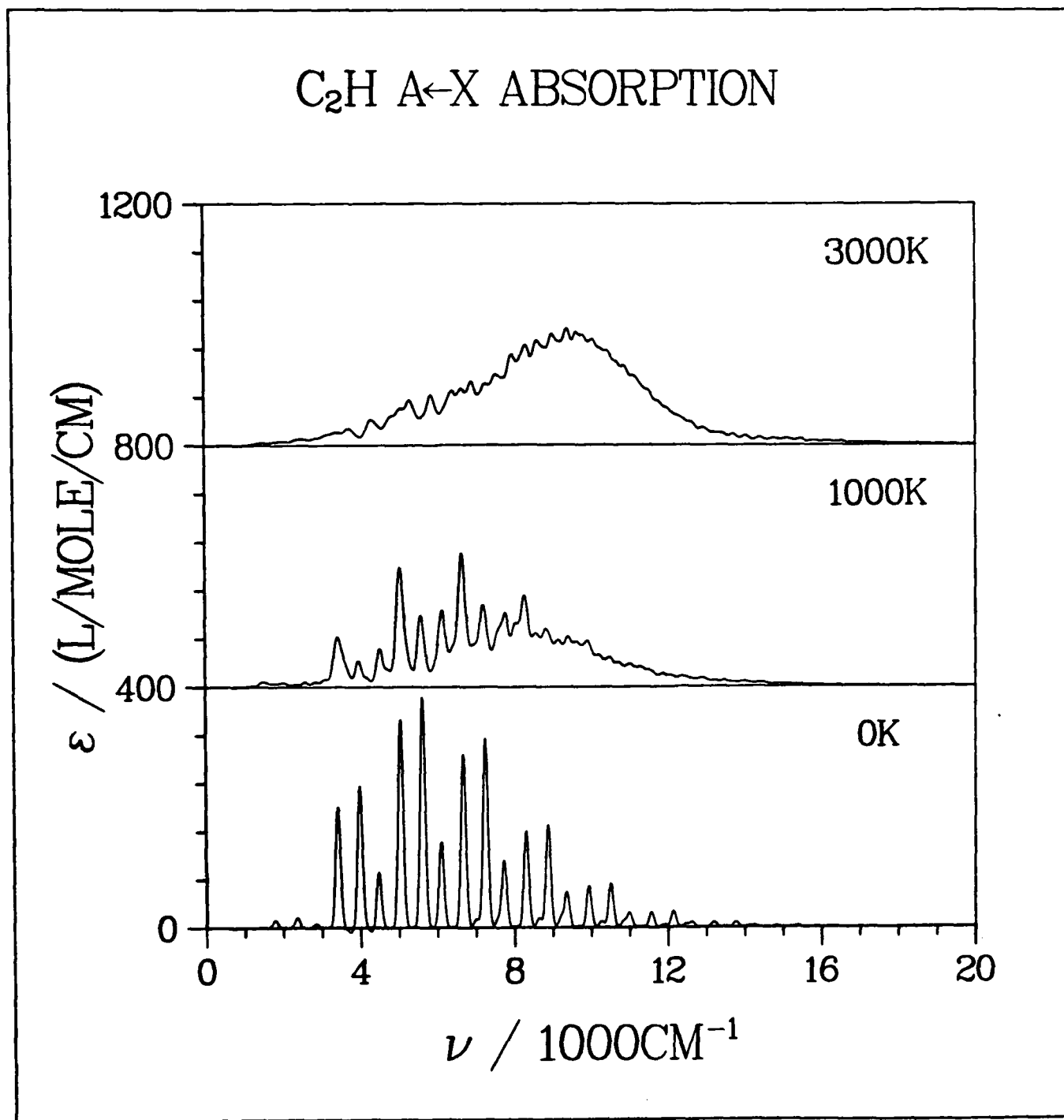


Figure 8. Total $A \leftarrow X$ Electronic Absorption Spectrum obtained by adding the individual $A(^2A') \leftarrow X$ and $A(^2A'') \leftarrow X$ spectra.

VI. CONCLUSIONS

This work is the first application of the high temperature spectral formalism of Reimers, Wilson and Heller²⁶ to either infrared spectra or the spectra of polyatomic molecules. The method is seen to be both simple and practical, requiring little more effort than pure classical mechanics. Some problems appear because of the use of frozen gaussians and classical temperatures but these fade in significance as the temperature is increased and the density of spectral lines increases. Also at high temperatures the dominantly bent character of the molecule reduces the effects of the Born Oppenheimer approximation, allowing the $A \leftarrow X$ absorption to be represented as the sum of the $A(^2A') \leftarrow X$ and $A(^2A'') \leftarrow X$ absorptions.

The C_2H potential surfaces have distinctive properties which are not characteristic of typical laboratory molecules like HCN. First C_2H is floppy, leading to large thermal bend displacements. When this couples with the appreciable mechanical anharmonicity and electrical non-linearity, many overtone and combination bands appear in the infrared spectra. Both the natures of the Fermi resonances involved and the energy level differences are seen to be important in redistributing intensity from the fundamentals to the overtones. In particular the CC stretch fundamental is predicted to get most of its intensity from anharmonic effects, and its intensity is predicted to be highly temperature dependent. The $A(^2A'') \leftarrow X$ electronic transition is relatively simple but the $A(^2A') \leftarrow X$ absorption is complicated by the large thermal motion and bend frequency disparity. We see many blue shifted hot bands with highly non-Boltzmann intensity distributions, and progressions in a mode that is not displaced. The center of the absorption band shifts 4000cm^{-1} to the blue when C_2H is heated from 0K to 3000K. Its intensity increases considerably due to the forbidden nature of the parallel transition, leaving the unaffected $A(^2A'') \leftarrow X$ band as a shoulder to the red of the $A(^2A') \leftarrow X$ band. A very large number of lines appear in the hot spectra and these blend into a continuum at 60cm^{-1} resolution.

Experimentally only the region $3500\text{--}4200\text{cm}^{-1}$, in the tail of the absorption band, has been investigated.¹⁵ Within this region the calculated intensity due to the electronic transitions (Figures 6-8) is much greater than the vibrational intensity (Figures 4-5). This supports the conclusions of Carrick, Merer and Curl¹⁵ that none of their observed bands in this region is primarily of vibrational nature. This work shows that the overall band structure contains a lot of information about the potential surfaces and therefore it is desirable that the entire band be experimentally observed in the gas phase.

We have shown that it is possible to calculate *ab initio* the often complicated spectra of small molecular fragments like C_2H . There exists many chemical species in this category, ranging from covalent second row type molecules to largely ionic molecules like NaOH and NaCl to fragments of transition metal complexes and clusters. In general these are difficult species to observe and characterize in the gas phase so that their spectra are difficult to obtain. Molecules of this type are important though as reaction intermediates and in astrochemistry, and they are often found at high temperature. It is hoped that the CASSCF and wave packet techniques used here will be of general use for predicting their spectra.

ACKNOWLEDGEMENTS

We thank the National Aeronautics and Space Administration, Ames Research Center; the Department of Energy; the National Science Foundation, Chemistry; and the Office of Naval Research, Chemistry for providing the support which made this work possible.

References

1. K. D. Tucker, M. L. Kutner, and P. Thaddeus, "The ethynyl radical C_2H - a new interstellar molecule," *Astrophys. J.*, vol. 193, p. L115 (1974).
2. A. Wootten, E. P. Bozayan, D. B. Garrett, R. B. Loren, and R. L. Snell, "Detection of C_2H in cold dark clouds," *Astrophys. J.*, vol. 239, p. 844 (1980).
3. A. Baudry, F. Combes, M. Perault, and R. Dickman, "Observation of millimeter wave emission from interstellar HCO^+ , HCN , and CCH ," *Astron. Astrophys.*, vol. 85, p. 244 (1980).
4. P. J. Huggins, W. J. Carlson, and A. L. Kinney, "The distribution and abundance of interstellar C_2H ," *Astron. Astrophys.*, vol. 133, p. 347 (1984).
5. T. Tsuji, "Abundance of molecules in the stellar atmosphere," *Ann. Tokyo Astron. Obs. Ser. 2*, vol. 9, p. 1 (1964).
6. S. Morris and A. A. Wyller, "Molecular dissociative equilibria in carbon stars," *Astrophys. J.*, vol. 150, p. 877 (1967).
7. A. H. Laufer, "Reactions of ethynyl radicals. Rate constants with CH_4 , C_2H_6 , and C_2D_6 ," *J. Phys. Chem.*, vol. 85, p. 3828 (1981).
8. J. H. Goebel, J. D. Bregman, D. M. Cooper, D. Goorvitch, S. R. Langhoff, and F. C. Witteborn, "The C_2H , C_2 , and CN electronic absorption bands in the carbon star HD 19557," *Astrophys. J.*, vol. 270, p. 190 (1983).
9. H. Okabe, "Photochemistry of acetylene at 1470\AA ," *J. Chem. Phys.*, vol. 75, p. 2772 (1981).
10. J. Grebe and K. R. Homann, "1982 Blue-green chemiluminescence in the system $C_2H_2/O/H$. Formation of the emitters $CH(A^2\Delta)$, $C_2(d^3\Pi_g)$ and C_2H ," *Ber. Bunsenges. Phys. Chem.*, vol. 86, p. 587 (1982).
11. S. T. Ridgway, "Jupiter: identification of ethane and acetylene," *Astrophys. J.*, vol. 187, p. L41 (1974).
12. W. R. M. Graham, K. I. Dismuke, and W. Weltner, Jr., " C_2H radical: ^{13}C hyperfine interaction and optical spectrum," *J. Chem. Phys.*, vol. 60, p. 3817 (1974).
13. M. E. Jacox, "Matrix isolation study of the vibrational spectrum and structure of HC_2 ," *Chem. Phys.*, vol. 7, p. 424 (1975).
14. R. Botter, V. H. Dibeler, J. A. Walker, and H. M. Rosenstock, "Experimental and theoretical studies of protoionization-efficiency curves for C_2H_2 and C_2D_2 ," *J. Chem. Phys.*, vol. 44, p. 1271 (1966).
15. P. G. Carrick, A. J. Merer, and R. F. Curl, Jr., " $A^2\Pi \leftarrow X^2\Sigma^+$ infrared electronic transition of C_2H ," *J. Chem. Phys.*, vol. 78, p. 3652 (1983).
16. J. Barsuhn, "Molecular calculations concerning a new candidate for the unidentified emission line at 89.190 GHz," *Astrophys. Letts.*, vol. 12, p. 169 (1972).
17. A. A. Reĭtlat, "Hyperfine splitting in the rotational levels of the C_2H molecule," *Sov. Astron. Letts.*, vol. 6, p. 406 (1980).
18. D. E. Milligan, M. E. Jacox, and L. Abouaf-Marguin, "Vacuum-ultraviolet photolysis of acetylene in inert matrices. Spectroscopic study of the species C_2 ," *J. Chem. Phys.*, vol. 46, p. 4562 (1967).
19. S. Shih, S. D. Peyerimhoff, and R. J. Buenker, "Theoretical prediction of the vertical electronic spectrum of the C_2H radical," *J. Molec. Spectrosc.*, vol. 64, p. 167 (1977).

20. H. Köppel, L. S. Cederbaum, and W. Domcke, "Strong nonadiabatic effects and conical intersections in molecular spectroscopy and unimolecular decay: $C_2H_4^+$," *J. Chem. Phys.*, vol. 77, p. 2014 (1982).
21. S. Shih, S. D. Peyerimhoff, and R. J. Buenker, "Calculated potential surfaces for the description of the emission spectrum of the C_2H radical," *J. Molec. Spectrosc.*, vol. 74, p. 124 (1979).
22. J. O. Arnold, D. M. Cooper, C. Park, and S. G. Prakash, "Line-by-line transport calculations for Jupiter entry probes," *Progress in Astronautics and Aeronautics*, vol. 69, p. 52 (1979).
23. D. M. Cooper and S. R. Langhoff, "A theoretical study of selected singlet and triplet states of the CO molecule," *J. Chem. Phys.*, vol. 74, p. 1200 (1981).
24. B. O. Roos, *Int. J. Quantum Chem.: Quantum Chem Symp.*, vol. 14, p. 175 (1980).
25. P. E. M. Siegbahn, J. Almlöf, A. Heiberg, and B. O. Roos, "The complete active space SCF (CASSCF) method in a Newton-Raphson formulation with application to the HNO molecule," *J. Chem. Phys.*, vol. 74, p. 2384 (1981).
26. J. R. Reimers, K. R. Wilson, and E. J. Heller, "A time dependent wave packet approach to thermal equilibrium systems: Electronic spectra," *J. Chem. Phys.*, vol. 79, p. 4749 (1983).
27. J. K. G. Watson, "The vibration-rotation hamiltonian of linear molecules," *Molec. Phys.*, vol. 19, p. 465 (1970).
28. G. D. Carney, L. A. Curtiss, and S. R. Langhoff, "Improved potential functions for bent AB_2 molecules: water and ozone," *J. Molec. Spectrosc.*, vol. 61, p. 371 (1976).
29. J. R. Reimers and R. O. Watts, "A local mode potential function for the water molecule," *Molec. Phys.*, vol. 52, p. 357 (1984).
30. E. J. Heller, "Frozen Gaussians: A very simple semiclassical approximation," *J. Chem. Phys.*, vol. 75, p. 2923 (1981).
31. T. H. Dunning, Jr., "Gaussian basis functions for use in molecular calculations. I. Contraction of $(9s\ 5p)$ atomic basis sets for the first-row atoms," *J. Chem. Phys.*, vol. 53, p. 2823 (1970).
32. S. Huzinaga, "Gaussian-type functions for atomic systems. I," *J. Chem. Phys.*, vol. 42, p. 1293 (1965).
33. T. H. Dunning, Jr., "Gaussian basis functions for use in molecular calculations. III. Contraction of $(10s\ 6p)$ atomic basis sets for the first-row atoms," *J. Chem. Phys.*, vol. 55, p. 716 (1971).
34. S. M. Adler-Golden, G. D. Carney, S. R. Langhoff, and C. W. Bauschlicher, "Theoretical calculations of ozone vibrational infrared intensities," *J. Chem. Phys.* (1984). submitted.
35. E. J. Heller, "Time-dependent approach to semiclassical dynamics," *J. Chem. Phys.*, vol. 62, p. 1544 (1975).
36. J. R. Reimers and E. J. Heller, "The exact eigenfunctions and eigenvalues of a two-dimensional rigid rotor obtained using gaussian wave packet dynamics," *Chem. Phys. Letts.* (1985). In preparation.
37. J. R. Reimers, K. R. Wilson, and E. J. Heller, "Infrared and electronic spectra of a diatomic dissolved in a liquid," *Chem. Phys. Letts.* (1985). In preparation.
38. P. J. Davis and I. Polonsky, "Numerical interpolation, differentiation and integration," in *Handbook of Mathematical Functions*, ed. M. Abramowitz and I. Stegun, Dover Publications, Inc., New York (1965).

39. E. J. Heller, "The semiclassical way to molecular spectroscopy," *Accts. Chem. Res.*, vol. 14, p. 368 (1981).
40. G. Simons, R. G. Parr, and J. M. Finlan, "New alternative to the Dunham potential for diatomic molecules," *J. Chem. Phys.*, vol. 59, p. 3229 (1973).
41. J. N. Huffaker, "Diatomic molecules as perturbed morse oscillators. I. Energy levels and II. Extension to higher order parameters," *J. Chem. Phys.*, vol. 64, p. 3175 and 4564 (1976).
42. A. R. Hoy, I. M. Mills, and G. Strey, "Anharmonic force constant calculations," *Molec. Phys.*, vol. 24, p. 1265 (1972).
43. F. B. van Duijneveldt, *IBM Research Report*, vol. RJ945 (1971).
44. S. R. Langhoff and E. R. Davidson, "Configuration interaction calculations on the nitrogen molecule," *Int. J. Quantum Chem.*, vol. 8, p. 61 (1974).
45. E. B. Wilson, Jr., J. C. Decius, and P. C. Cross, *Molecular Vibrations*, McGraw-Hill, New York (1955).
46. R. D. Coalson and M. Karplus, "Extended wave packet dynamics: Exact solution for collinear atom, diatomic molecule scattering," *Chem. Phys. Lett.*, vol. 90, p. 301 (1982).
47. W. Domcke, H. Köppel, and L. S. Cederbaum, "Spectroscopic effects of conical intersections of molecular potential energy surfaces," *Molec. Phys.*, vol. 43, p. 851 (1981).
48. J. P. Bergsma, P. H. Berens, K. R. Wilson, D. R. Fredkin, and E. J. Heller, "Electronic spectra from molecular dynamics: A simple approach," *J. Phys. Chem.*, vol. 88, p. 612 (1984).
49. S.-Y. Lee and E. J. Heller, "Exact time-dependent wave packet propagation: Application to the photodissociation of methyl iodide," *J. Chem. Phys.*, vol. 76, p. 3035 (1982).
50. E. J. Heller, E. B. Stechel, and M. J. Davis, "Molecular spectra, Fermi resonances, and classical motion," *J. Chem. Phys.*, vol. 73, p. 4720 (1980).
51. D. R. Fredkin, A. Komornicki, S. R. White, and K. R. Wilson, "Ab initio infrared and Raman spectra," *J. Chem. Phys.*, vol. 78, p. 7077 (1983).
52. D. A. McQuarrie, *Statistical Mechanics*, Harper and Row, New York (1976).
53. P. H. Berens and K. R. Wilson, "Molecular dynamics and spectra: I. Diatomic rotation and vibration," *J. Chem. Phys.*, vol. 74, p. 4872 (1981).

END

FILMED

8-85

DTIC